*Review Article*

# Influence of Deposition Parameters for Cu₂O and CuO Thin Films by Electrodeposition Technique: A Short Review

**E. Arulkumar,[1] S. Thanikaikarasan ⓘ,[1] and Nega Tesfie ⓘ[2]**

[1]*Department of Physical Sciences, Saveetha School of Engineering, Saveetha Institute of Medical and Technical Sciences, Chennai 602105, Tamil Nadu, India*
[2]*Department of Mechanical Engineering, Faculty of Manufacturing, Institute of Technology, Hawassa University, Hawassa, Ethiopia*

Correspondence should be addressed to Nega Tesfie; negat@hu.edu.et

The transition metal oxide-based nanomaterial attracted researchers for its various applications due to its interesting physical, chemical, and optical properties. Copper oxide thin films with different oxidation states were prepared on various transparent, nontransparent nature conducting substrates from the acidic and alkaline medium by electrodeposition technique. The deposition parameters such as potential, bath temperature, solution pH, and deposition time determine the physical, chemical, and optical properties. The complexing agents such as sodium thiosulfate, lactic acid, citric acid, and triethanolamine determine the stability of cuprous and cupric ions in the deposited films. Optical properties reported that the deposited films have direct band gap value 1.3 and 3.7 eV represents the absorbance of the deposited films in the visible region of solar spectrum. The absorbance of light in visible region, good electrical conductivity, and various nanostructure morphologies with the environment-friendly constituents are the distinctive properties of copper metal oxides.

## 1. Introduction

Developing the synthesis routes for nanoparticles and nanostructures constitutes the majority of research in the subject of nanotechnology in its entirety. Such efforts allowed for the creation of nanomaterials with various compositions, monodisperse crystallite sizes, novel crystalline forms, and complex construction features. As a result, transition metal oxides (TMO's) are compounds of oxygen atoms that bond with transition metals. Subsequently, it must be easily oxidized and tuned their components in different oxidation states which makes the reactions of redox systems and also it is doped with trivalent and pentavalent impurities found in various applications by the synthesis of formation of nanoparticles [1–3], nanoclusters [4, 5], quantum dots [6], nanorods [7], nanotubes [8], nanofibers [9], nanowires [10, 11], nanofilms [12, 13], and nanoflowers [14]. Despite all the size of the nanoparticles can be controlled in their dimensions and particle size up to 100 nm by different synthesis processes. The majority of synthesis approaches were discovered empirically, i.e., through experiments and they represent solitary attempts

without any basic ideas or mechanistic principles that would permit a logical synthesis approach. Consequently, the properties of nanoparticles are controlled with a large surface area to volume ratio, high-ionic nature, low porosity, high luminescence, high photoabsorbance, superior catalytic activity along with semiconducting properties. Transition metal oxide nanoparticles have unique properties with their applications in biological and optoelectronic devices. As a result, the nanoparticles with a pair of positively and negatively charged ions just like the human's umbilical vein, endothelial cell [15]. Given that positively charged metal oxide nanoparticles are more effective than negatively charged metal oxide nanoparticles for biological applications and that positively charged nanoparticles have an enhanced capacity for the adsorption of plasma proteins and interaction with antibodies, serum proteins, and other molecules [16, 17]. Positively charged nanoparticles have a higher rate of mineralization in human breast cancer compared to negatively charged nanoparticles [18]. The surface area of the metal oxide nanoparticle has tremendous absorbance behavior enhancing the photocatalytic mechanism related to charge separation and electron-hole recombination

for photoelectrochemical [19], antibacterial [20], and antimicrobial [21] effects by developing radicals. The adsorption and desorption of the TMO's were adjusted by its ionic conductivity. The TMO's were found to exhibit better pseudo capacitance behavior because of its tunable semiconductor with electronic configuration, accessibility, and reversibility between variable oxidation states. The crystalline, amorphous nature, morphology, surface area, and hydrated water content determine capacitance of the energy storage. The transition metal oxide structure exhibits the electrochemically stable charge discharge cycles [1, 22, 23]. The process of doping and capping agent's results in tailoring of suitable surface morphology with dimensions found applications in biological, photocatalytic, and solar cells [24, 25]. The process of tailoring has been obtained by the process of requirement for several applications. Recently, several researchers worked on transition metallic elements such as Ti [26, 27], Cr [28], W [29, 30], Mn [31], Fe [32–34] Co [35–37], Ni [38], Pt [39], Cu [40], Ag [41, 42], and Au [43]. The copper transition metal is low-cost materials and it is ideal for physical and chemical preparation techniques compared to transition metals viz., Ti, Cr, W, Pt, Ag, and Au. The technique of electrodeposition is found to be simple, low cost, low temperature, less time consuming, large surface to volume ratio, the stoichiometry of the deposited films can be controlled by the adjustment of deposition parameters such as solution pH, bath temperature, potential, and concentration of the electrolytic bath. The present review focused the review about electrochemical synthesis of copper oxide thin films such as copper (I) oxide (cuprous) and copper (II) oxide (cupric). The role of deposition parameters such as potential, bath temperature, and solution pH value from the previously observed results were reported.

## 2. Basic Properties of CuO and $Cu_2O$

There are two types of copper oxides, such as cuprous oxide (CuO) and cupric oxide ($Cu_2O$), different in colors, that is, red and black. Cuprous oxide and copper oxide with molecular formula CuO and $Cu_2O$ crystallized in cubic structure with covalent in nature. It can be reduced when it is subjected to higher temperature above 35°C. The ratio of proportion of copper in acidic solutions produced $Cu^{2+}$ and $Cu^+$ ions. $Cu_2O$ or CuO decomposed to release oxygen if it is heated and acts as oxidant in the reactive composites and looping of chemical combustion. The process of heating produced metallic copper from CuO and it converted into to $Cu_2O$ [44]. CuO found to exhibit corrosion resistance as a result of interaction between copper and oxygen in the air to produce protective oxide in the form of thin layers covers the substrate. Usually, CuO with oxidation number having higher value is found to be thermally more stable than $Cu_2O$. CuO is not soluble in organic and inorganic solvents; however, it is dissolved in the solution of ammonia [45]. The structure of CuO is monoclinic, whereas the structure is found to be cubic in electrodeposition [46, 47]. The influence of density, which takes into account both media and particle components determines the density of nano agglomerates in the liquid suspension. The standard unit for specific volume in the SI system is cubic meters per kilogram, whereas its

values are 6.31 and $6.0\,g\,cc^{-1}$ for CuO and $Cu_2O$, respectively [48]. In case of solid state, a band gap is also called an energy gap is in the range of energy present in a solid where no other electronic states can exist. The band gap is generally denoted as the energy difference in the band structure of the solids in both insulators and semiconductors. The ability of a hole to move through a metal or semiconductor, in the presence of an applied electric field is called hole mobility. As a result, the hole mobility of both $Cu_2O$ and CuO is −250 and $0.1–10\,ms^{-1}V^{-1}$, respectively [49].

*2.1. Highlights of Copper Transition Metal Oxides.* The enhancement of Cu nanoparticles are practically important due to its various biological applications viz., bacteriostatic agents, fungicides at low temperature, and production from low-cost precursors compared with Ag, Au, Cu, and Pt nanoparticles. The process of doping pentavalent and trivalent impurities with copper is easy due to the reason of diffusion on the substrates in addition with oxidation states of copper viz., $Cu_2O$ and CuO. The gap between valence and conduction band plays a vital role in semiconductors, since the oxides exhibit optical properties with indirect band gap values between 2.5 and 3.7 eV for $Cu_2O$ (cuprite). The band gap value of CuO (tenorite) is between 1.3 and 1.8 eV which can absorb 50% of photons within the visible region of the solar spectrum between 300 and 620 nm. Copper is a soft, malleable, and ductile metal with very high thermal and electrical conductivities because copper can be hammered or out of shape forever. So, its surface area is suitable for the behavior of absorbance of visible light. Copper material is used for many low-cost energy conversion devices. Copper has been used in most of the electronic devices due to its electrical conductivity. Since, there are a lot of electrons carry flow of current in solar cell applications. Nowadays, the copper electrode has been used in high-capacity Li-ion batteries. Moreover, $Cu_2O$ is also known for its catalytic activity at low temperature toward the oxidation of organic compounds. Copper nanoparticle enhances photocatalytic applications and realistic competitor for biological applications viz., bacteriostatic agents, fungicides at low temperature, and low-cost precursors compared with Ag, Au, and Pt nanoparticles [26–30, 50].

## 3. Electrodeposition of CuO and $Cu_2O$

Electrodeposition is the process that involves the growth of cationic and anionic precursors on the surface of transparent and nontransparent nature conducting substrates. In this process, an electric current passes through the electrochemical cell that consists of working, counter, and reference electrodes. The schematic arrangement of the experimental setup for the electrochemical process is shown in Figure 1. In this method the applied potential on the working electrode in the electrolytic bath consists of cations and anions where the deposit is formed. There is a requirement of a counter electrode to complete the electrical circuit and the reference electrode to provide the standard input potential of the electrode. The ions in the electrolytic bath attracted toward the surface of the working electrode by the application of an external electric field. The anions are deposited on a cathodic
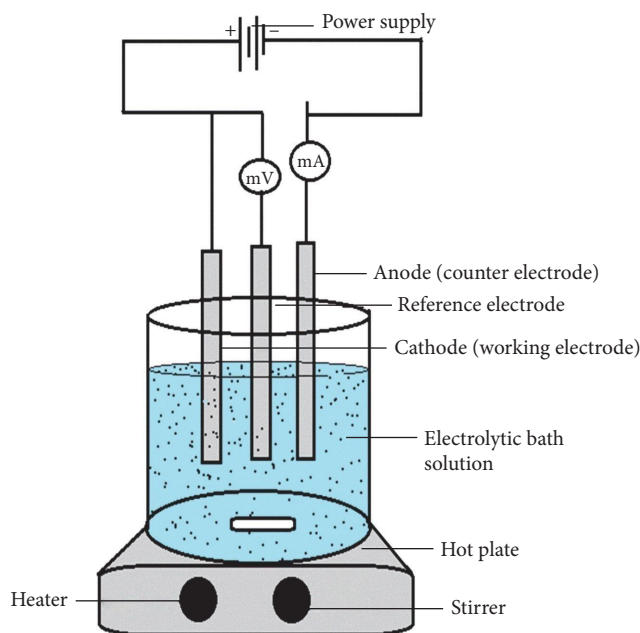
FIGURE 1: Representation of experiment setup for the preparation of $Cu_2O$ and CuO thin films by electrodeposition method.
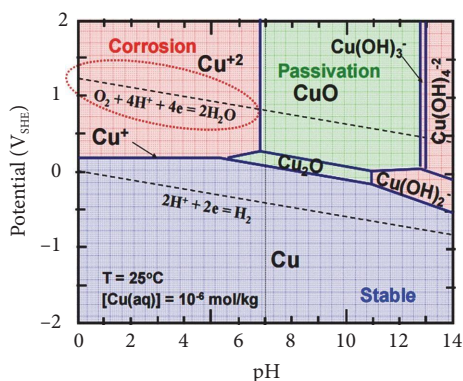


FIGURE 2: Pourbaix diagram for Cu in an aqueous solution at 25°C.

metallic substrate which is called cathodic electrodeposition, whereas the cations deposited on an anodic metallic substrate is named as anodic electrodeposition. In cathodic electrodeposition the $OH^-$ ions produced on the metallic substrate neutralizes the positive ions which are deposited on the substrate. In an anodic electrodeposition, the oxidation occurs on the metal part, which has been neutralized by the negative ions and the ions are deposited on the metallic surface on the working electrode. Several researchers focused the growth of $Cu_2O$ and CuO thin films which have been reported earlier. The influence of various substrates such as stainless steel, indium tin oxide (ITO), platinum for $Cu_2O$, and CuO thin films was reported earlier [12, 47, 50–68]. The source of chemicals used were copper acetate ($Cu(CH_3COO)_2 \cdot H_2O$)) [18], copper sulfate pentahydrate ($CuSO_4 \cdot 5H_2O$) [51], cupric nitrate trihydrate ($Cu(NO_3)_2 \cdot 3H_2O$) [53, 54], and cupric chloride dihydrate ($CuCl_2 \cdot 2H_2O$) [52] for the preparation of precursors. The solubility of Cu is not stable thermodynamically in water
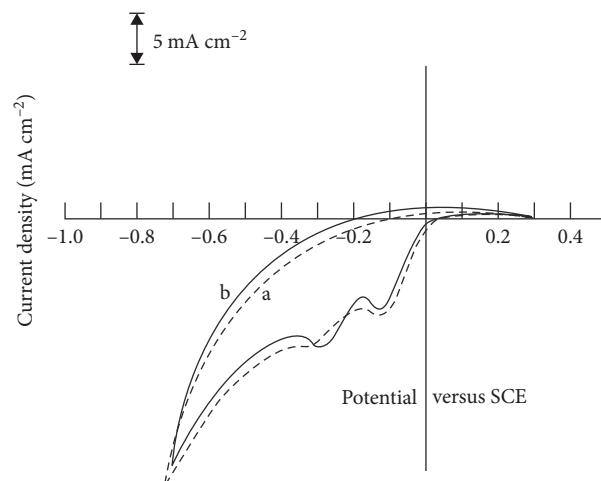


FIGURE 3: Voltammograms of $Cu_2O$ on (a) copper (–): (b) tin oxide coated glass (-) in 0.45 M $CuSO_4$, 3.25 M of lactic acid and NaOH. Scan rate: 20 $mVs^{-1}$; solution pH: $9.0 \pm 0.1$.

in the presence of oxygen as reported by Brandt et al. [55]. The dependence of solubility for $Cu^{2+}$ and $Cu^+$ ions with different temperature, various solution pH values with different potential was explained using Pourbaix diagram is shown in Figure 2 [56]. The generation of $Cu_2O$ with high oxidation mostly takes place in the range of solution pH values in between 6.0 and $12.0 \pm 0.1$.

## 4. Electrochemical Growth Mechanism of $Cu_2O$ and CuO

The deposition potential influences the film growth, structure, surface morphology with nanosize, and weight percentage of the material deposited as layer on the substrate. Growth mechanism of $Cu_2O$ film on tin oxide coated glass substrate by electrodeposition was carried out by the technique of cyclic voltammetry. The electrolytic bath consists of 0.45 M $CuSO_4$ in addition with 3.25 M lactic acid with few drops of NaOH as denoted in Figure 3 [69]. The range of potential in between 0.5 and −1.0 V versus SCE with peak potential at −180 mV versus SCE which correspond to the reduction of copper according to Equation (1):

$$Cu^{2+} + e^- \longrightarrow Cu^+. \tag{1}$$
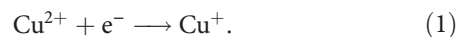
The appearance of cathodic peak at −0.35 versus SCE, which could be explained by the formation of $Cu_2O$ on the substrate according to Equation (2). The primary electrochemical reaction involved in the growth of $Cu_2O$ film incorporated with the Faraday's laws of electrolysis:

$$2Cu^+ + 2OH^- \longrightarrow Cu_2O + H_2O, \tag{2}$$

$$2Cu^{2+} + 2e^- + H_2O \longrightarrow Cu_2O + 2H^+. \tag{3}$$
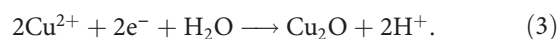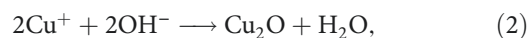
In the electrodeposition of $Cu_2O$ reduction of $Cu^{2+}$ ions to $Cu^+$ for Equation (4) and the precipitation of $Cu^+$ ions to
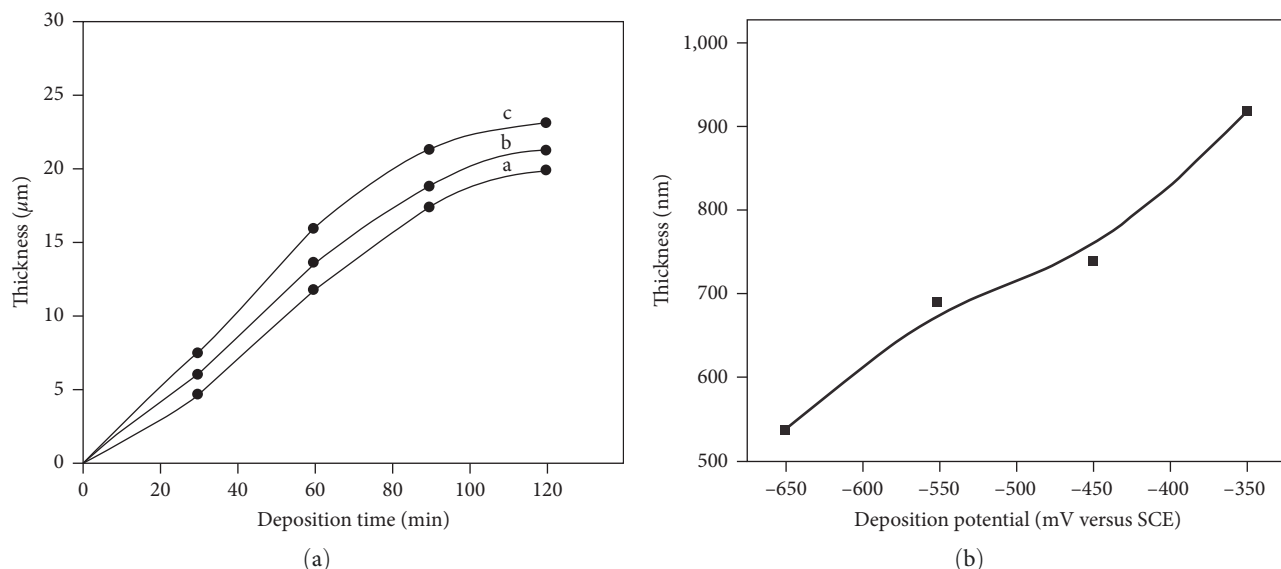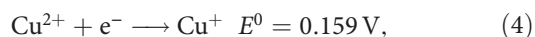
(a)



(b)

FIGURE 4: Variation of film thickness with various potential (a) $Cu_2O$: −0.355, −0.455, −0.555 V versus SCE. Solution pH $9.0 \pm 0.1$ bath temperature 70°C. (b) CuO: −350, −450, −550, and −650 mV.

$Cu_2O$ due to the solubility of $Cu^+$ ions limited according to the following equations [70]:

$$Cu^{2+} + e^- \longrightarrow Cu^+ \quad E^0 = 0.159\,V, \tag{4}$$

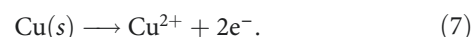$$2Cu^{2+} + H_2O + 2e^- = Cu_2O + 2H^+. \tag{5}$$

In the cyclic voltammetry of $Cu_2O$, an electrode immersed in the Cu (II) acetate solution is slightly acidic. The observation of cathodic and anodic in the potential range between 660 and 1,000 mV versus SCE. The appearance of anodic peak at 530 mV versus SCE corresponds to the dissolution of $Cu_2O$ to $Cu^{2+}$ according to Equation (6).
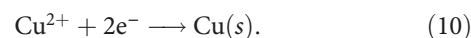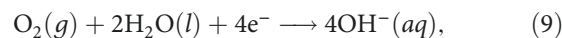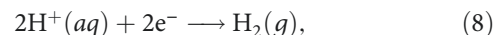
The current was gradually increased concerning the cathodic potential, which determines the growth rate of $Cu_2O$. Consequently, the growth of $Cu_2O$ thin film on copper and tin oxide substrates was analyzed using a cyclic voltametric pattern leading to selecting an optimum potential in the range between −0.3 and −0.6 V [69]. The formation of $Cu_2O$ film is homogeneous in thickness with the appearance of reddish gray when deposited on Cu and tin oxide substrates. As a result, the deposition time was fixed at 2 hr to obtain the requirement of uniformity with higher thickness value. Figure 4(a) shows the variation of film thickness with deposition time with different potential, denoted by three lines indicated as shown in figure. But when the deposition potential increases, the film's uniformity decreases and its look like spotted. Therefore, the optimum potential for the development of $Cu_2O$ thin films is 550 mV against SCE. Similar to this, it was discovered that the variation in thickness was correlated with the variation in deposition potentials 0.355, 0.455, and 0.555 V and its value is in the range between 2 and 2.3 μm. The concentration of $OH^-$ ions and the solution pH rise as the partial pressure of oxygen in the solution bath rises; results an increase in the deposition potential. By establishing a relationship between the charge (Q) transmitted and

the mass (M) of the deposited material, a graph of the number of electrons (n) transferred for the creation of single molecule $Cu_2O$ [71]. The slope of the resulting straight line gave $n = 2$, indicating that the process of electrodeposition produced stoichiometric $Cu_2O$. Furthermore, several researchers reported that the electrochemical deposition of cupric oxide thin films is carried out potentiostatically from an aqueous acidic bath containing $CuSO_4$ and L (+) tartaric acid [53, 54, 72, 73]. If oxygen is present in deionized water, it consumes that the excess of electrons produced by the dissolution of Cu with anodic and cathodic reactions which can take place according to Equation (7).

In anodic surface:

$$Cu(s) \longrightarrow Cu^{2+} + 2e^-. \tag{7}$$

In the cathodic metallic surface:

$$2H^+(aq) + 2e^- \longrightarrow H_2(g), \tag{8}$$

$$O_2(g) + 2H_2O(l) + 4e^- \longrightarrow 4OH^-(aq), \tag{9}$$

$$Cu^{2+} + 2e^- \longrightarrow Cu(s). \tag{10}$$

The dissolution rate of Cu in $H_2O$ depends upon the parameter value such as temperature, solution pH, and the concentration of dissolved oxygen present in the electrolytic bath [57, 58]. The electrodeposition of CuO on ITO substrate with different potential values were reported [69]. The electrolytic bath consists of equal molar ratio (0.03 M) of copper sulfate ($CuSO_4$) and L (+) tartaric acid and the deposition potential was fixed in the range of potential in −0.350 and −0.650 V within the step increment of 100 mV with respect to SCE. The electrolytic bath was kept at 75°C and the deposition process was taken out for 30 min. Thickness of the

deposited films was estimated using Stylus Profilometer (Mitutoyo SJ 301). The formation of $Cu^{2+}$ carried out potentiostatically in an alkaline medium leads to produce CuO thin thus represent the following equation:

$$CuSO_4 \longrightarrow Cu^{2+} + SO_3^{2-} \quad (E^0 = 0.34\,V). \tag{11}$$
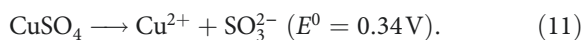
When the flow of direction of current through the electrochemical cell, simultaneous formation of $Cu^{2+}$ ions and $OH^-$ ions on the surfaces of the anode and cathode. Subsequently, both ion react with one another to make $CuSO_4$ and then hydrate $Cu(OH)_2$ leads to produce CuO.

$$SO_4^{2-} + H_2O + 2e^- \longrightarrow 2OH^- + SO_3^{2-} \quad (E^0 = -0.94\,V), \tag{12}$$

$$Cu^{2+} + 2OH^- \longrightarrow Cu(OH)_2, \tag{13}$$

$$Cu(OH)_2 \longrightarrow Cu^{2+} + 2OH^-. \tag{14}$$
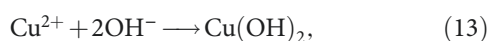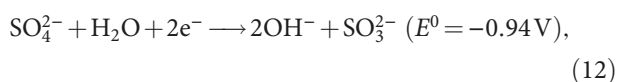
The production of $OH^-$ ions in both Equations (9) and (14) locally enhances the pH value at the interface and the formation of $Cu(OH)_2$ spontaneously which is suppressed by the addition of precipitation agents like NaOH, KOH, and $NH_4OH$ [70]. Subsequently, the $OH^-$ ions react with the metallic copper at pH value $9.0 \pm 0.2$ which results in the formation of CuO. Equation (15) directs the electrodeposition approach to produce CuO thin films [69]. $CuSO_4$ molecules are forced to separate from their metastable state in this process, producing cupric oxide at a pH value around $13 \pm 0.1$. Finally, the reaction produces a coating of cupric oxide on the substrate.

$$Cu^{2+} + 2OH^- \longrightarrow CuO + H_2O. \tag{15}$$
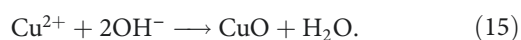
The variation of film thickness with potential is represented for CuO is shown in Figure 4(b). The increase in the value of deposition potential leads to a steady state with an increase in film thickness, which may lead to a higher deposition rate. It has been reported that film thickness affects microstructural and optical properties [74–76]. The film thickness should be adjusted for the device sizes in microelectronic applications. Therefore, it is vital to investigate the change of CuO microstructure with thickness value; however, it changes the physical properties. The other essential parameter is electrodeposition like bath temperature and time of deposition was kept constant. It is noted that film thickness increases with potential linearly. Similar observations for CuO thin films have been reported earlier by Dhanasekaran et al. [47]. The observed results show that the deposition of CuO film thickness increases because the increase in deposition time could be attributed to a rise in the mobility of adatoms with a longer deposition time. This could consequently increase the crystallite and grain size or other related effects, increasing film thickness reported with various deposition potential values reported by Sayem Rahman et al. [77]. The deposition of CuO film with various potential −0.45, −0.55, and −0.65 V. The deposition

potential −0.45 and 0.65 V linearly increases for film thickness with potential above −0.65 V. The film thickness is increased suddenly by the consequent increment of deposition of atoms. The deposition of nanocrystalline thin films on various substrates found several applications photovoltaic, photoelectrochemical, and fuel cells [78–80]. The deposition parameters such as solution pH, bath temperature, and potential values which determine the structure, surface morphology, composition as well as optical properties.

*4.1. Bath Temperature.* The bath temperature plays a very significant role in thickness, size, plane orientation as well as crystallinity of the deposited films [47]. The increase in value of bath temperature from low to higher, whereas the decrease in quantity of the particles. The reduction of internal stress found to increase in value of crystallite size of the deposited films. The stress is more important parameter influenced by the current density depends upon the temperature [81]. The effect of polarization is another advantage of the higher temperature. The type of polarization originates from change in electrolyte concentration carried out by the flow of current through the electrode-solution interface is known as concentration polarization. As a result, the electrochemical cell potential difference differs from its equilibrium value. The diffusion of thin films and increase in value of ionic diffusion as the temperature increases. This may be due to the diffusion of thin layers and its value increase if the temperature rises, whereas reduction of concentration polarization. On the other hand, at higher temperature the increase in value of energy consumption provided heat for bath evaporation. Additionally, strains will manifest at high processing temperatures and can produce a major effect, particularly thermal expansion coefficient of the coating is different from the substrate temperature [82]. Therefore, it is preferable to plate at a high temperature that maximizes coating quality by the usage of minimum energy. The deposition of thin films in this technique takes place in the temperature range in between room temperature and 90°C. Initially bath temperature around 35°C the time of deposition found to be higher due to the slow rate of release of ions from the electrolytic bath. The deposition takes place in the intermediate temperature range 40–70°C, the rate of release of ions is found to be higher thus results films with well adherence to the substrate leads to producing films with higher thicknesses and well-defined crystallinity. This may be due to the fact that diffusion of ions takes place quickly and the rate of deposition increases leading to produce the film with a higher thickness value. If the bath temperature is found to rise above 80°C the electrolytic bath takes place the status of evaporation, and the results decrease in value of current density producing films with a lower thickness which may be due to peel off of the film from the substrate [59, 83–87]. As a result, the temperature was fixed between 40 and 80°C to obtain films with higher thicknesses and well-defined crystallinity. The growth of CuO thin films at various temperatures between 45 and 90°C was reported by Dhanasekaran et al. [47]. The deposition of CuO thin films with a much lower temperature of 10°C with step increments of 10°C up to slightly higher

temperatures above 40°C was reported by Keikhaei and Ichimura [60]. The preparation of Cu₂O thin films at various temperatures between 40 and 60°C was reported by Benhaliliba et al. [61].

*4.2. Solution pH.* The solution pH value is one of the important parameter determine highly the structure and sizes of the particles. So, the effect of pH on the incorporation of particle is dependent on the nature of the particles. So many researchers concluded that increase in pH value found to decrease the amount of particles present in the coatings [88]. The decrease in value of pH is preferred to maintain the internal stress in the deposited films. In this case pH values found to be less than $5.0 \pm 0.1$, to obtain an acceptable range of stress in the deposited films. An increase in the pH value of the solution may lead to the discharge of hydroxyl ions instead of dissolution and oxygen evolution [89] resulting in a high value of internal stress. The deposition of Cu₂O thin films at various acidic solution pH values between $2.4 \pm 0.2$ and $5.8 \pm 0.2$ was reported by Keikhaei and Ichimura [60]. The electrochemical growth of Cu₂O thin films at various alkaline solution pH values between $9.5 \pm 0.2$ and $12.5 \pm 0.2$ has been reported by Rahal et al. [54] and Jrajri et al. [90]. Consequently, the solution pH value changes the surface morphology, composition, and corrosion like properties. The complexing agents with their adjustment in between the range of solution pH $2.0 \pm 0.2$ and $4.0 \pm 0.2$ there is a possibility of the slow rate of hydrogen evolution. In contrast, the higher pH values increase the development of hydrogen. The range of solution pH value film in between $2.5 \pm 0.2$ and $3.5 \pm 0.2$ leads to produce films with smooth surface and microcracks. The formation of microcracks is not associated with hydrogen but rather the formation of different phases, crystallographic nature, and lattice parameters. But, there is a slight variation in pH values that changes the surface with microcracks and the sizes of the grains. The pH value changes the distribution of electrons in the outer shell and also the concentration of the elements present in the deposited films [51, 62, 68, 91–100].

*4.3. Potential.* In electrodeposition potential plays a significant role there is a passage of least potential into the electrolyte cell to produce thin films in the level microscopically [90]. The production of Cu²⁺ or Cu⁺ ions depend upon the concentration of the electrolyte with smallest applied potential. Jiang et al. [62, 100] reported the various deposition potentials with step increment of −150 mV versus SCE in the range −100−−900 mV [94]. The equilibrium electrode potential of reduction and oxidation are described by using the Nernst relation obtain the capacity of Cu²⁺ and Cu⁺ ions take place reduction with condition equal to the standard electrode potential at 298 K with atmospheric pressure.

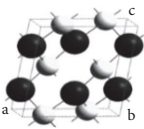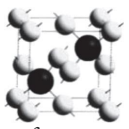$$E = E_0 + \frac{[RT]}{[nF]} \ln \frac{[Ox]}{[Red]}, \tag{17}$$

where $E$ is the potential of the working electrode in the given electrolytic solution, $E_0$ is the standard electrode potential, $R$ is a universal gas constant, $T$ is the absolute temperature of

the electrolytic bath, $N$ is the number of electrons required for the reduction, and F is the Faraday constant. In this equation ions occur electrode reduction potential from standard electrode reduction potential for an ion measured [5, 95]. And also, the deposition potential able control accurately the fact such as current density, over potential, reactant concentration at the electrode interface (e.g., hydrodynamic) [96]. Therefore, the electrochemical performance for the rate of ions mass transfer depends on potential. In this case, the higher potential causes higher mass transfer rate with comparative higher electrochemical performance and lower potential vice versa for higher potential. So, in the electrodeposition method, the bath temperature, solution pH, and deposition potential are those three factors that affect structural and morphology features. The properties of cuprite and tenorite are shown in Table 1.
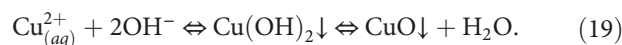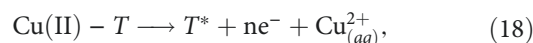
# 5. Structural Properties

The electrodeposited Cu₂O thin films found to exhibit cubic structure with various solution pH values in between 9.51 and $12.5 \pm 0.1$ [90] and different bath temperature in the range 40–70°C [81], various substrate such as stainless steel and SnO₂ [83], finally different potential in between −0.4 and −0.6 V [97] is shown in Figure 5(a)–5(d). In this case the bath temperature plays a significant role in determine the crystallinity and structure. If the temperature is quite low, there is the growth of tiny metallic crystals. The electrolytic bath temperature was kept in between 40 and 70°C for Cu₂O deposited on the fluorine tin oxide (FTO) substrate. The $2\theta$ values found at 29.36, 36.5, 42.4, 52.5, 61.5, 65.7, and 73.6 are corresponding to (110), (111), (200), (211), (220), (221), and (222) planes, respectively (Figure 5(c)) with cubic structure (ICDD File No. 75–1531). The peak with the highest intensity (111) represents the preferential orientation of crystal by its comparison with other planes. The diffraction peaks FTO does not observed in the XRD pattern. This may be due to the reason that Cu₂O layers deposited on FTO have densely packed to the substrate. Moreover, the intensity of the Cu₂O was slightly decreased due to the growth direction of the Cu₂O film changed form (111) to (220) plane by the temperature increased from 55 to 70°C. In addition when that the bath temperature increased above 80°C there is evaporation of electrolytic bath take place resulting decrease in thickness value of the deposited films. So, we concluded the bath temperature has a significant low on the film growth as a result, the crystallinity decreases with increase of bath temperatures and the bath temperature of 40°C is favorable for obtaining high Cu₂O crystalline thin film [82]. Figure 5(a) represents the XRD pattern of Cu₂O with variation of alkaline pH in between 9.5 and $11.5 \pm 0.1$ and the values exhibit Cu₂O (111) plane orientation with metallic Cu peaks. But, the pH value $12.5 \pm 0.1$ does not allow Cu₂O phase and the $2\theta$ values which is corresponding to metallic copper phase [77]. As a result, the change of solution pH value modified the structural properties of Cu₂O. The structural properties of Cu₂O thin films on transparent and nontransparent nature conducting substrates was reported by Thanikaikarasan et al. [83] and the XRD

TABLE 1: General properties of cuprite and tenorite.

| Properties | CuO (tenorite) | Cu$_2$O (cuprite) |
|---|---|---|
| Crystal structure |  The special atomic positions for copper are (1/4, 1/4,0); (3/4,3/4,0); (1/4,3/4,1/2); (3/4,1/4,1/2) and for oxygen are (0,y,1/4); (1/2,1/2+y,1/4); (0,y,3/4); (1/2,1/2−y,3/4) with y = 5 0.416(2). Copper atoms are represented by small light spheres and oxygen atoms are represented by large dark sphere |  The atomic positions for copper are (0,0,0); (0,1/2, 1/2); (1/2,0,1/2); (1/2,1/2,0) and the tetrahedral sites positions (1/4,1/4,1/4) and (3/4,3/4,3/4) for oxygen. Copper atoms are represented by small light spheres and oxygen atoms are represented by large dark spheres |
| Melting point (K) | 1,599 | 1,505 |
| Density (g cc$^{-1}$) | 6.31 | 6.0 |
| Stable phase | Monoclinic | Cubic |
| Band gap (eV) | 1.22–1.55 | 2.0–2.4 |
| Hole mobility (cm$^2$ V$^{-1}$s$^{-1}$) | 0.1–10 | −250 |
| Oxidation states | +1 | +2 |
| Space group | C$_2$c | Pn3m |
| a (Å) | 4.685(0) | 4.269(2) |
| b (Å) | 3.430(3) | - |
| c (Å) | 5.139(3) | - |
| β | 99.08(6)° | - |
| V/Z (Å)$^3$ | 20.64(8) | 38.89(9) |
| R$_e$ | 2.19% | 1.37% |
| R$_{wp}$ | 5.13% | 6.94% [54, 59, 62–65] |

pattern is shown in Figure 5(b). From this figure, the crystallites are referentially oriented along the (111) and (211) plane for the deposited films on SnO$_2$ and SS substrates. Because the height of the peak is higher than all other peaks in the diffractogram. As a result, the intensity of (111) and (211) plane is varied with respect to the substrate, determining the crystallite size, dislocation density, and strain due to the restoring force acting on the surface of the substrate. Figure 5(d) demonstrates the XRD pattern of Cu$_2$O thin film with various deposition potentials in between −0.4 and −0.6 V deposited on the FTO substrate. XRD pattern indicated the Cu$_2$O peaks are polycrystalline nature with cubic structure and the four FTO substrate peaks are obtained. Moreover, other phases such as CuO and metallic Cu are not observer by the variation of potential. As a result, the prominent (111) plane's intensity rises and strong with increase of deposition potential at 0.5 and 0.6 V. The full width at half maximum (111) plane is small, and the calculated crystallite size of Cu$_2$O at −0.4, −0.5, and −0.6 V versus SCE is 47, 94, and 80 nm, respectively [98]. Moreover, the structural properties of CuO thin films with deposited parameters such as bath temperature, solution pH value, substrate nature, and potential which has been reported earlier [54, 84, 96]. Few researchers reported that the electrodeposition leads to the formation of CuO by the role of reducing agent L (+) tartaric acid [95]. The formation of CuO is found to be less stable, just slightly lower at aqueous media, whereas the oxidation of Cu$^{2+}$ to Cu$^{3+}$ which has been obtained by the process of decomposition through the chemical route. The observation of the monoclinic structure

with C$_2$c space group was reported by Poizot et al. [50]. As a result, the formation of CuO is less stable than aqueous medium since the solubility with reducing agent plays the role to determine the crystalline structure of CuO according to that below mentioned Equation (19):

$$Cu(II) - T \longrightarrow T^* + ne^- + Cu^{2+}_{(aq)}, \tag{18}$$

$$Cu^{2+}_{(aq)} + 2OH^- \Leftrightarrow Cu(OH)_2\downarrow \Leftrightarrow CuO\downarrow + H_2O. \tag{19}$$

Mahmood et al. [98] analyzed the formation of CuO thin films with lower particle size depending upon the electrolyte concentration with deposition time. Initially, the electrodeposition of CuO takes place with addition of complexing agents such as dihydroxyacetone, dimethyl carbonate, glyceraldehyde, lactic acid, and trioxanes. The process of mass transfer in liquid takes place to migrate the ions from the copper electrolyte to the cathodic surface. The phases Cu$_2$O and CuO are more stable but there is observation of no structural phases in addition with the impurities. The rapid conversion of CuO from Cu$_2$O at higher temperature 550°C is denoted in Figure 6 [68, 90]. The deposition parameters such as bath temperature and deposition potential with respect to time and solution pH values determine the structural properties of CuO. In this case Figure 7(a) demonstrates that the XRD pattern of electrodeposited CuO thin films at various bath temperatures in between 45 and 90°C

(a)



(b)



(c)



(d)

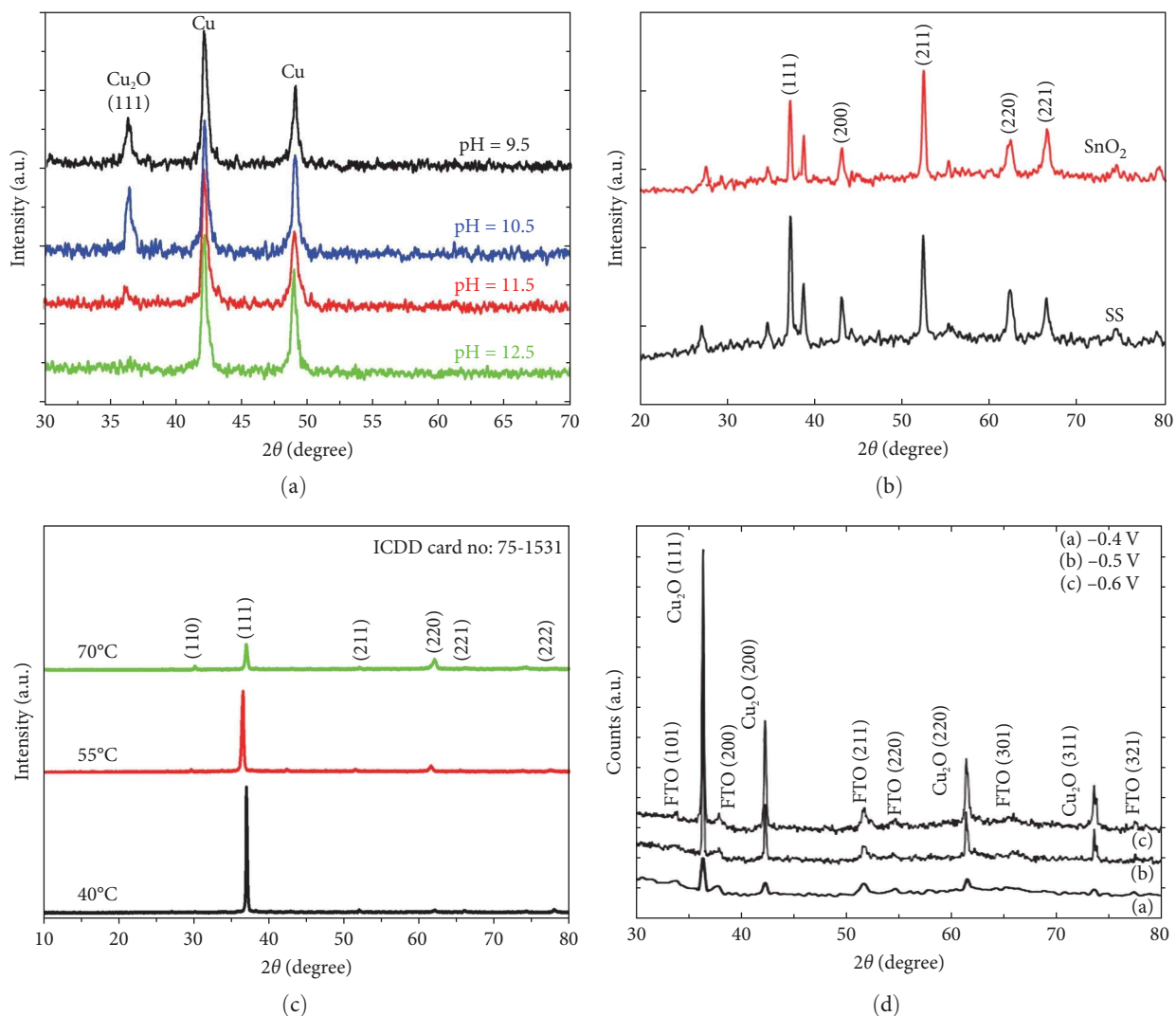FIGURE 5: X-ray diffraction patterns of electrodeposited $Cu_2O$ thin films at various: (a) solution pH values ($9.5 \pm 0$, $10.5 \pm 0.1$, $11.5 \pm 0.1$, and $12.5 \pm 0.1$), (b) stainless steel and $SnO_2$ substrate, (c) bath temperature (40, 55, and 70°C), and (d) deposition potential (−0.4, −0.5, and −0.6 V).
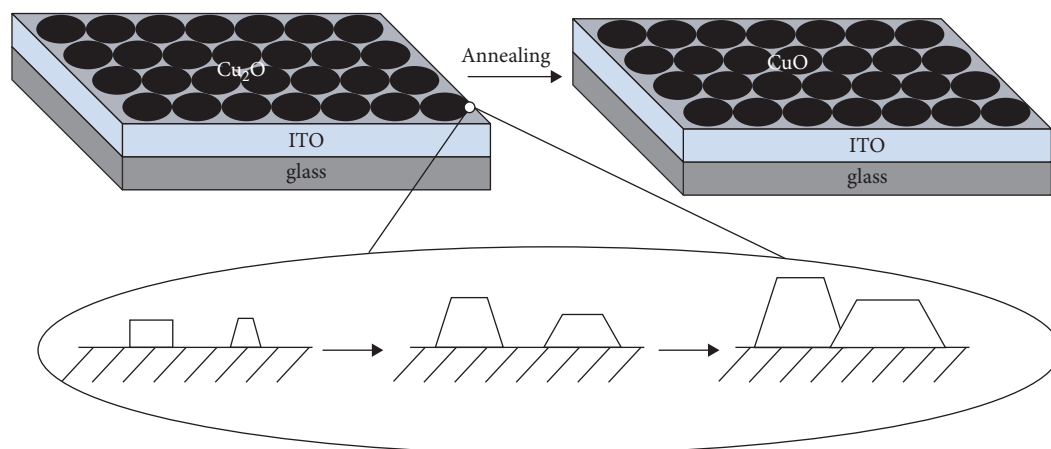


FIGURE 6: Schematic diagram of rapid conversion process for $Cu_2O$ to CuO at 550°C.
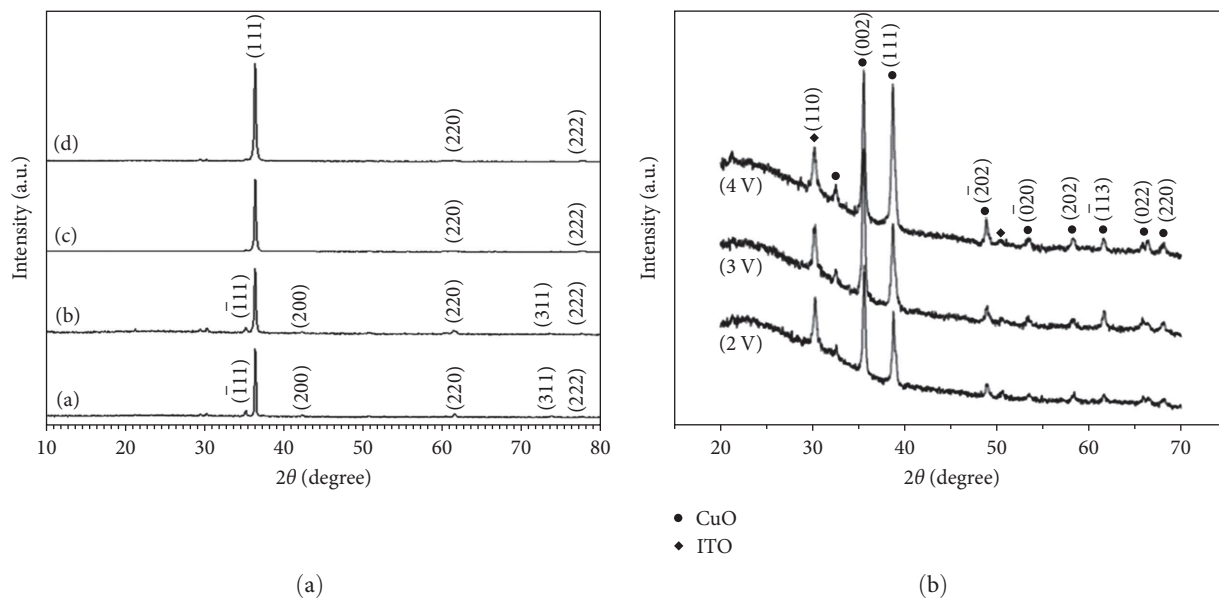
FIGURE 7: X-ray diffraction patterns of electrodeposited CuO thin films at various: (a) bath temperature: (i) 45°C, (ii) 60°C, (iii) 75°C, and (iv) 90°C: (b) with different potential: (i) 2 V, (ii) 3 V, and (iii) 4 V.
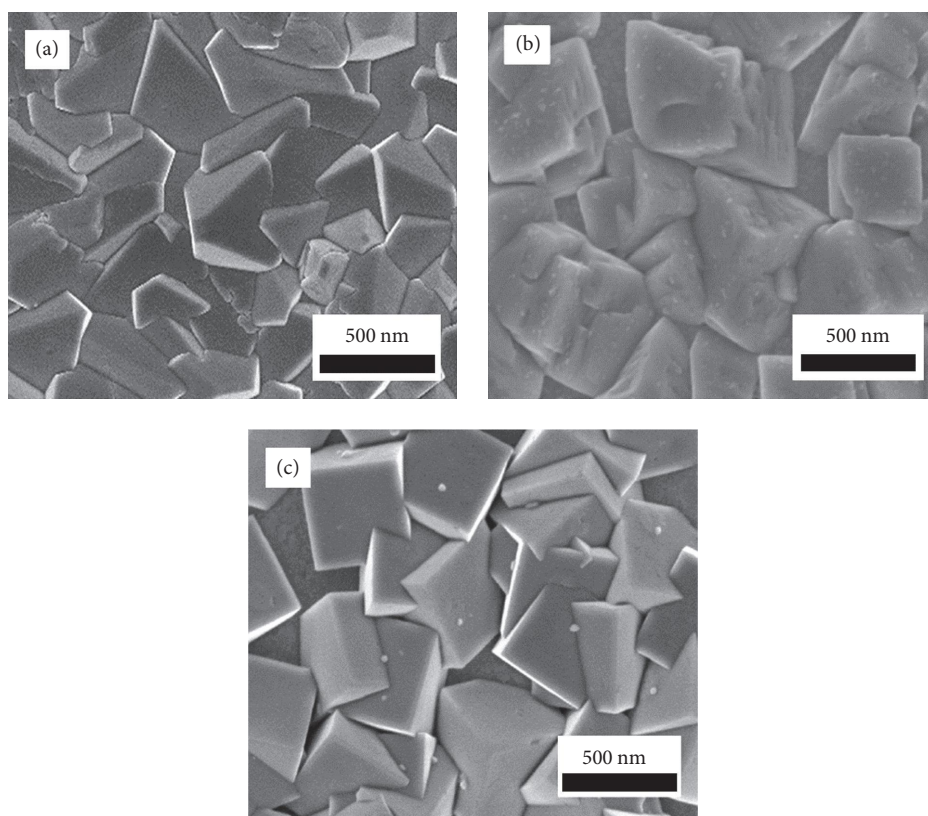


FIGURE 8: SEM images of electrodeposited $Cu_2O$ microcrystallites on indium tin oxide substrate with different complexing agents: (a) lactic acid, (b) citric acid, (c) EDTA [67].

on ITO substrate was reported by Dhanasekaran et al. [73]. Thickness of the CuO thin film linearly increases with respect to various bath temperatures and time and tends to attain saturation after 40 min of deposition. In this case, the thickness value increases quickly within 10 min due to

the presence of more ions in the electrolyte bath. Therefore, the deposited film is cubic phase with polycrystalline in nature along with preferred orientation (111) direction and peak position is found at $2\theta$ value around 36.43. Moreover, the (111) plane intensity is found to be very high with cubic

Cu$_2$O grain with (200)
preferred orientation

Cu$_2$O grain with both
(200) and (111)
preferred orientations

Cu$_2$O grain with (111)
preferred orientation



The stability constant of complexing agent decreases the overpotential decreases →

The growth of <111> orientation is impeded →

FIGURE 9: Schematic diagram of Cu$_2$O grains with different preferential orientation.



FIGURE 10: FESEM images for electrodeposited CuO thin film with various deposition time on indium tin oxide substrate postannealed at 550°C for 120 min. (S1) 300, (S2) 600, (S3) 1,200, and (S4) 1,800 s.
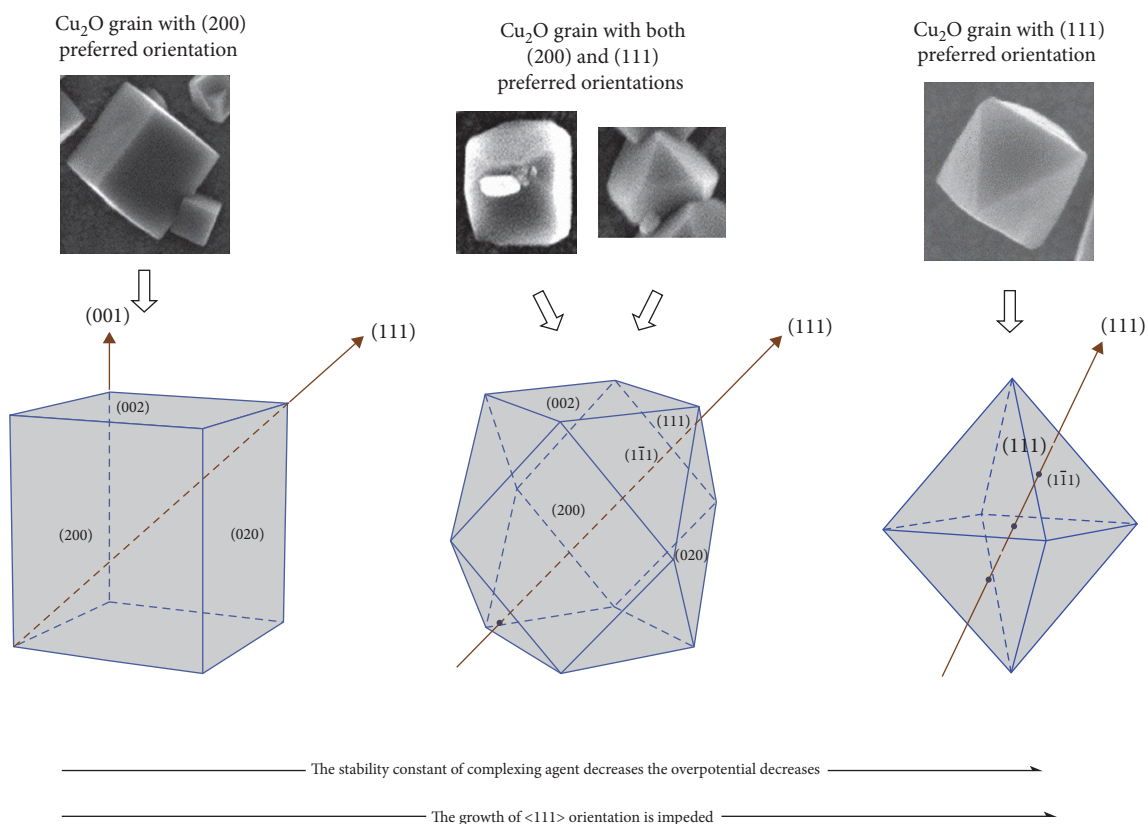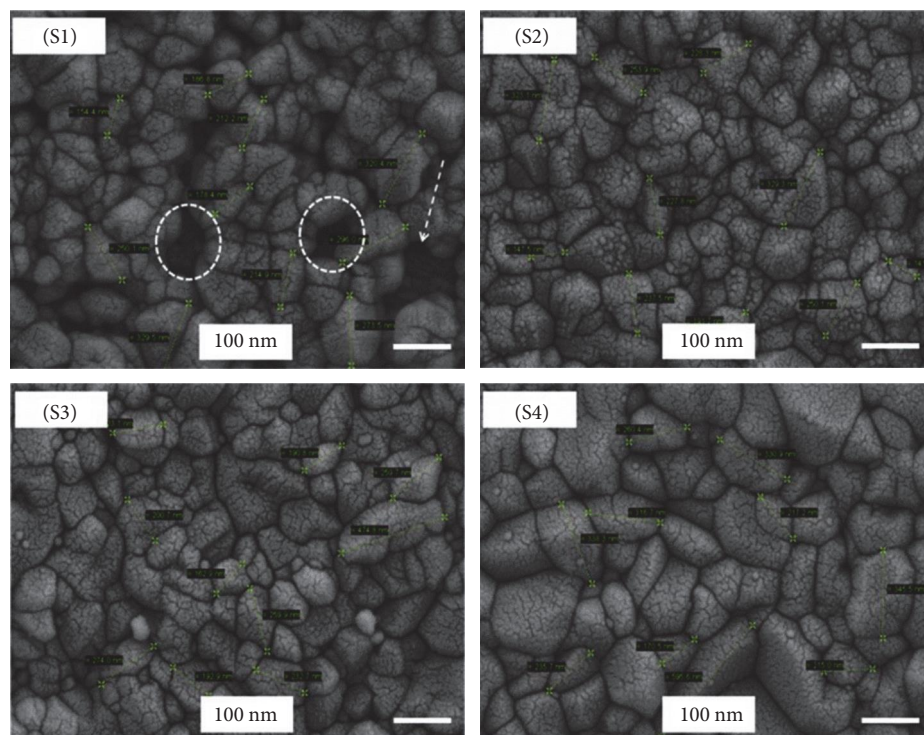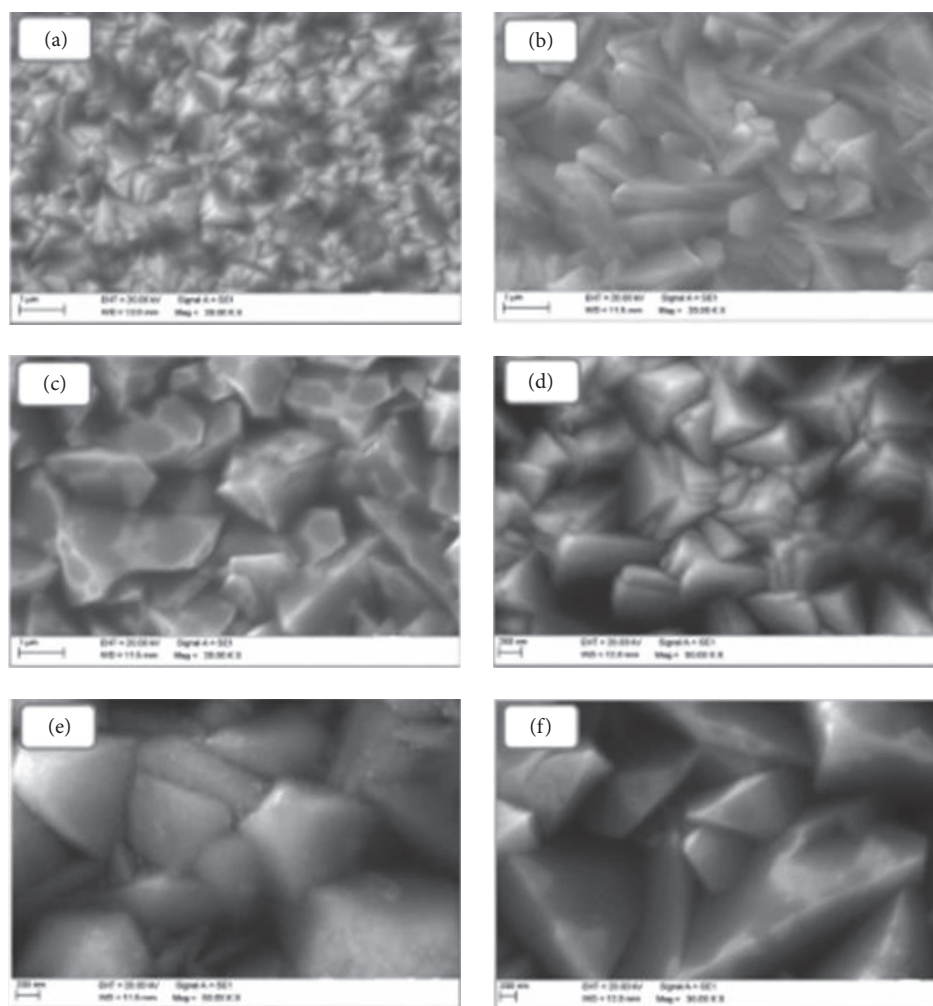
FIGURE 11: SEM images of electrodeposited Cu$_2$O thin films at various bath temperature with different magnification: 40°C (a, b), 55°C (c, d), and 70°C (e, f).

phase at bath temperatures as high as 90°C. But, in opposition, the CuO thin films formed at lower bath temperatures (45 and 60°C) produced monoclinic peaks (111) and (311) with higher intensities. As a result, the CuO have mixed phase formation when prepared at bath temperatures of 45 and 60°C, and they tend to transition of single phase creation for films deposited at 75 and 90°C [47]. Figure 7(b) shows the XRD pattern of CuO film with respect to various deposition potentials in between 2 and 4 V on the ITO substrate at 60°C [68]. As result all the diffraction peaks are indexed with monoclinic phases of CuO (JCPDS No. 05-0661) and the major peaks located at $2\theta$ value 35.54 and 38.70 are indexed as (002) and (111) crystal planes, respectively. The diffraction peaks rise when the deposition voltage is raised from 2 to 3 V, indicating how the crystallinity and size of CuO nanocrystals have improved. The diffraction peak for the (111) plane has a dramatically increasing intensity at 4 V deposition voltage. This implies that CuO films' morphologies will alter as the direction of crystal formation in this plane becomes more favorable. In addition, the spectrum's widening of all recorded peaks suggested that the presence of nanoscale crystallites [99].

## 6. Morphology

The morphological feature of copper oxide thin films depends upon the deposition parameters such as potential, solution pH, and bath temperature. The change of solution pH value determines the shape and size of the grains over the entire surface of the substrate. The effect of solution pH and deposition potential for Cu$_2$O thin films prepared on different substrates was reported earlier [65, 79]. Ma et al. [66] and Zhang et al. [67] investigated the role of complexing agents such as lactic acid, citric acid, and EDTA which is shown in Figure 8(a)–8(c) [66, 67]. The Cu$_2$O films electrodeposited with complexing agent citric acid found to exhibit preferential orientation along (111). Also, the films complexed with lactic acid are found to exhibit the most prominent reflection along (111) plane. Zhang et al. [67] reported that Cu$_2$O films addition with EDTA exhibit prominent reflection (200) along the surface of the substrate as Figure 9. Microscopic images of CuO deposited on ITO substrate at different time intervals in between 5 and 40 min as shown in Figure 10. The observation denoted that there is an agglomeration of thin film layer on the substrate by the process of mass migration from the
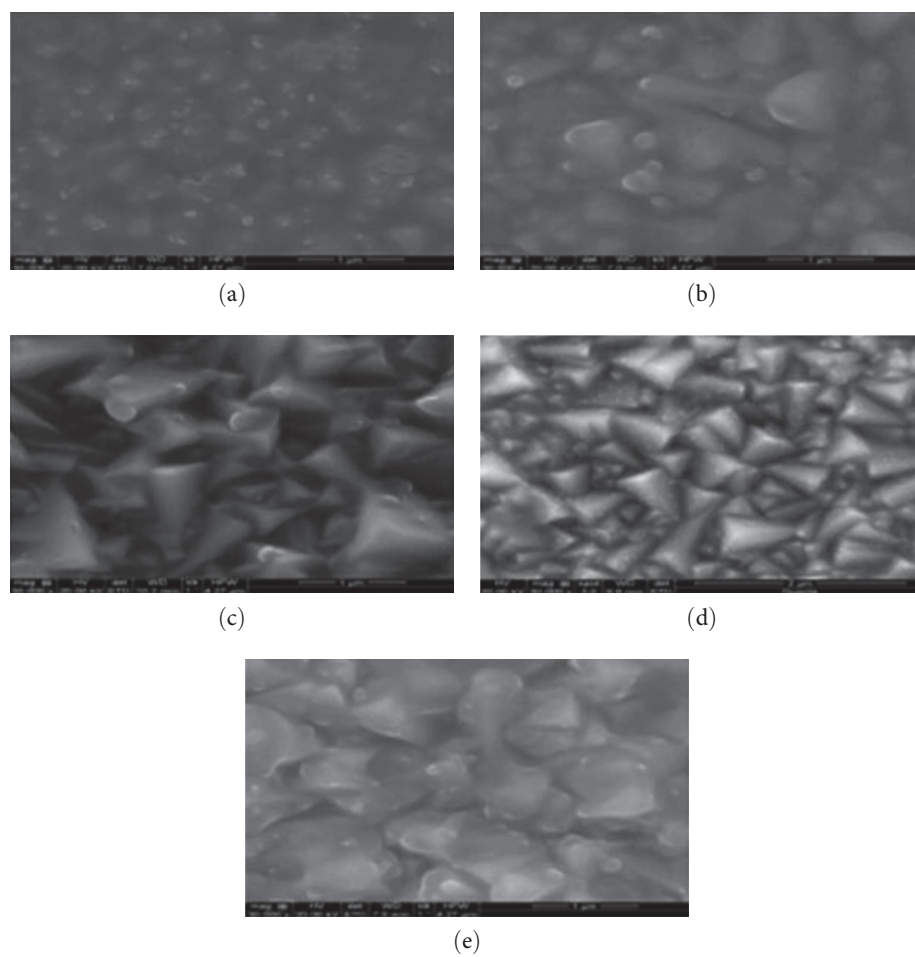
(a)



(b)



(c)



(d)



(e)

FIGURE 12: SEM images of CuO films electrodeposited at various bath temperature (a) 30, (b) 45, (c) 60, (d) 75, and (e) 90°C.
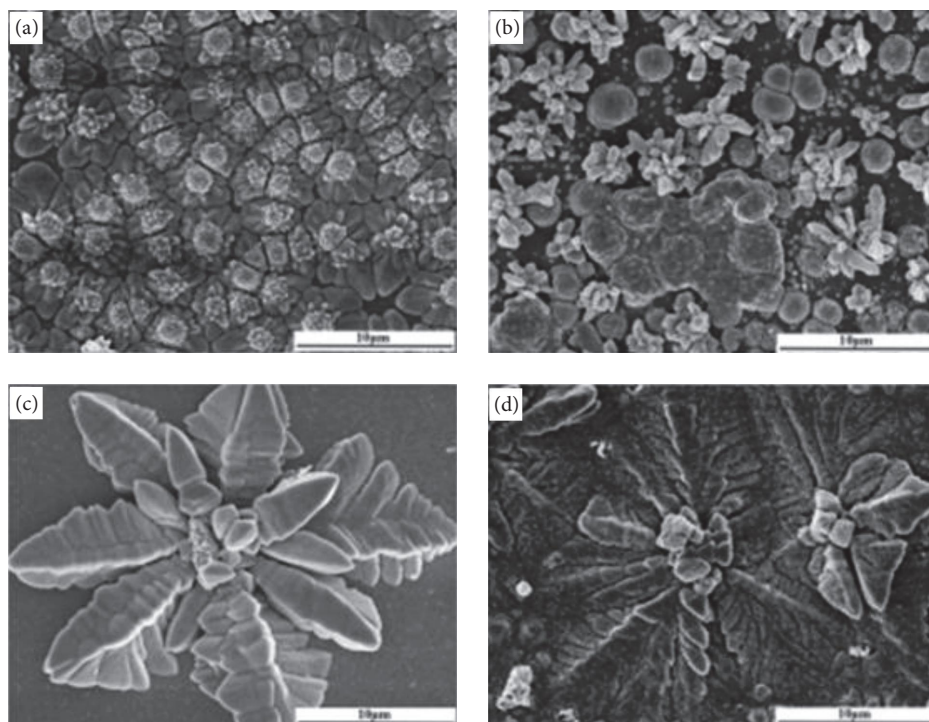


FIGURE 13: FESEM images of CuO films prepared at potential 3 V at various bath temperature (a) 20, (b) 40, (c) 60, and (d) 80°C.
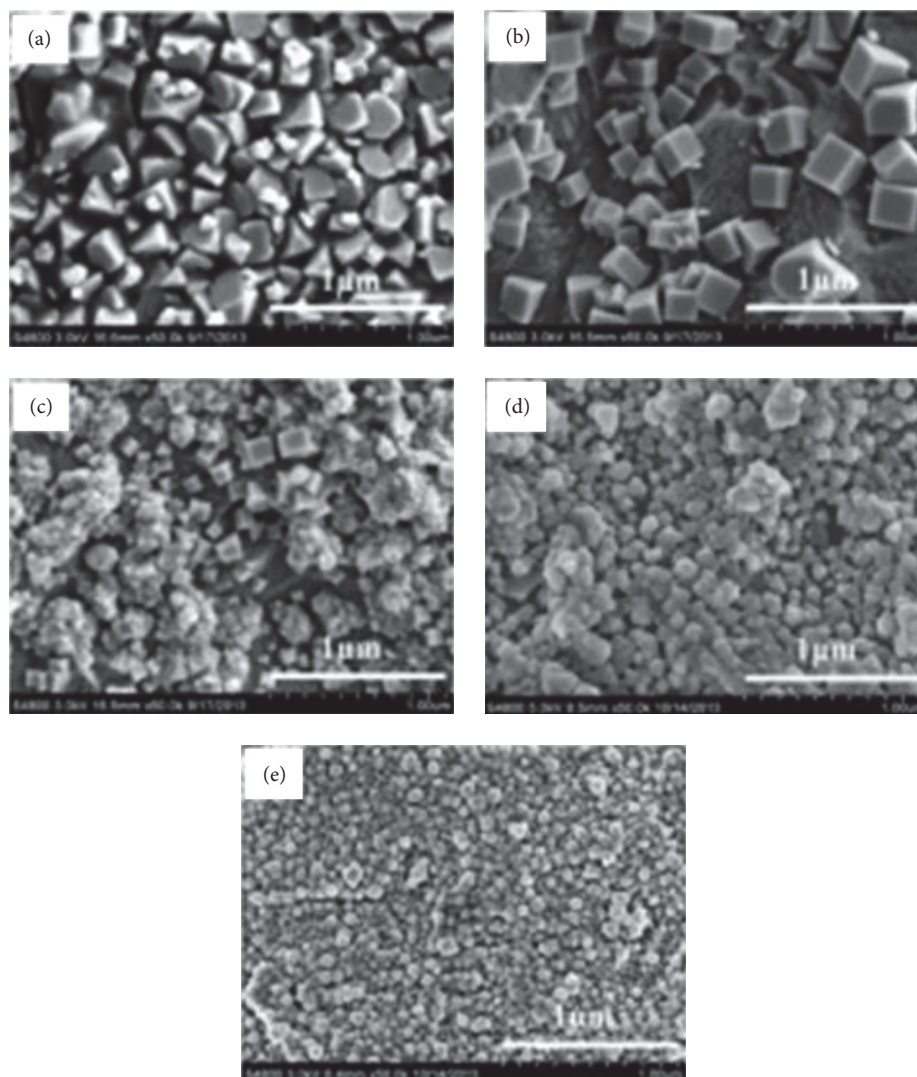
FIGURE 14: SEM images of Cu$_2$O thin films electrodeposited at various potential values: (a) −0.1, (b) −0.3, (c) 0.5, (d) −0.7, and (e) −0.9.

electrolytic bath. The films annealed at 550°C there is an agglomeration process which produces different sizes of particles with respect to deposition time. So, the influence of deposition time in electrodeposited CuO films the agglomeration condition plays a major role with respect to deposition time. At the same time the rate of reaction is found to be difficult to produce a film for a long-time interval due to the reason of consumption and evaporation from the electrolyte. The film with higher thickness leads to a change of stress which produces a crack in the deposited films. Resolution per minute changes the diffusion speed of the electrolyte and the growth rate of the crystal orientation. The process of postannealing temperature was found to be lower, there is a formation of inflorescence like morphology with smooth petals. Further increase of annealing temperature above 400°C there is extension of petals from its initial stage where as annealing temperature was found to be 600°C grains or smaller are grouped together with large grains. This observation result discussed that annealing temperature determines the crystallinity CuO thin films. The effect of temperature for Cu$_2$O thin

film prepared in the temperature range between 40 and 70°C is shown in Figure 11(a)–11(f) [81]. It is observed that the growth of the grains found to exhibit a distinctive three-sided pyramid structure with surface of substrate have well-defined crystallinity (Figure 11(a)–11(e). The distribution of grains with its size ~0.74 $\mu$m at temperature below 40°C is shown in (Figures 11(a) and 11(b). The growth of grain in pyramidal shape disordered at 55°C and the size of the grains increased up to 1.66 $\mu$m which is is shown in Figures 8(c) and 8(d). However, the bath temperature increased continuously above 70°C that the grains with pyramid shape found to reject with agglomeration into a corner truncated octahedral as shown in Figures 11(e) and 11(f) [82]. The average size of the grains increases upto 2.88 $\mu$m as a result of faster nucleation caused by electrodeposition at higher temperature, which favors the development of larger grains [99]. These observed results indicated that the bath temperature is very important to control the morphology of the electrodeposited Cu$_2$O films [100]. The analysis of surface morphology for electrodeposited CuO thin films within the range of temperature in between 30 and
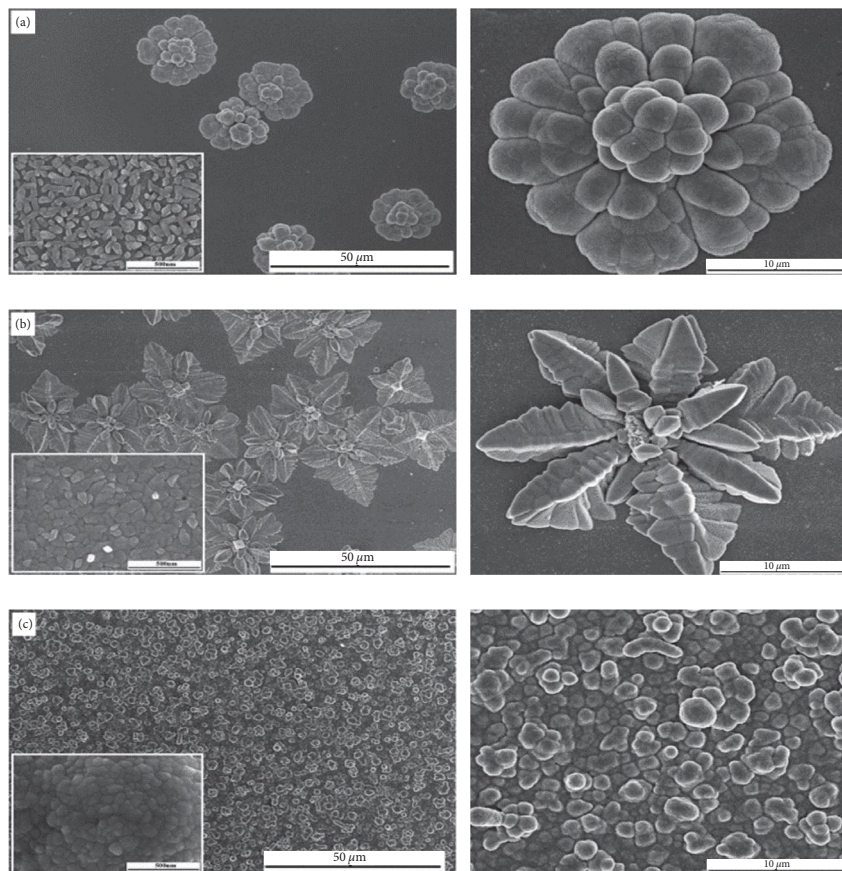
FIGURE 15: The FESEM images of CuO thin films prepared at 60 with 10 min for different potential values: (a) 2, (b) 3, and (c) 4 V for CuO films.

90°C is shown in Figure 12(a)–12(e). It is noted that the observation of pyramid-shape background with amorphous nature grains covered the entire surface of the film and no well-defined grain boundaries. The bath temperature at 30°C found to exhibit slightly amorphous nature, not uniform morphology and also surface discontinuity was observed as shown in Figures 12(a) and 12(b). Similarly, the bath temperature at 45°C also have grains with different sizes in between 100 and 150 nm without the appearance of grain boundaries (Figure 12(c)). The appearance of well-defined pyramid-shaped grain with crystalline nature and the presence of stress in the deposited films which may be due to coalescence of grain boundaries is shown in (Figure 12(d)). The deposition of CuO film with bath temperature at 75°C exhibited to uniform surface. It is noted that the deposited films in between 40 and 75°C found to exhibit well-defined morphology. The smaller grains are grouped together to frame a larger grains with size value in between 200 and 300 nm. Finally, the bath temperature reaches around 90°C denoted the grains with different sizes in presence of grain boundaries not visible (Figure 12(e)). It has also been reported that the cluster of smaller grain with large size but at higher bath temperature diffuses the shape of the grains. The regular arrangement of atoms by the placement of stress plays much intention on the layer coating of cupric oxide. The average size of the grains found to be in the range between 300 and 400 nm. As a result,

we have concluded that the electrolytic bath temperature modified the surface properties due to the reason of increase in bath temperature leads to the enhancement of mobility of the surface. The morphological feature of CuO thin films with respect to bath temperature in between 20 and 80°C were reported by Wang et al. [68]. The observed results reported that the bath temperature found to be lower, results the formation of intense grain with uniform distribution on the substrate as shown in Figures 13(a) and 13(b). It is noted that there is formation of CuO particles with fine and symmetric nature on the substrate takes place at the temperature around 60°C which is shown in Figure 13(c), whereas the temperature reaches 80°C the morphology is observed to be nonuniform with rough surface which is denoted in Figure 13(d). This may be due to the reason that there is a growth rate of grains with sediment nature in which the increment of temperature up to a certain level. Thereafter, the decrease of bath temperature found to decrease the process of cathodic polarization which makes the ions with much activation energy and diffusion velocity. By the same time there is a reduction of polarization with internal stress leads to the formation of films with good quality. However, the increase of bath temperature can also accelerate the nucleation rate which makes the electrodeposited layers with cracks. The stirring speed also changes the morphology of CuO deposited layers with dendritic branches largely reducing the sizes of the grains which
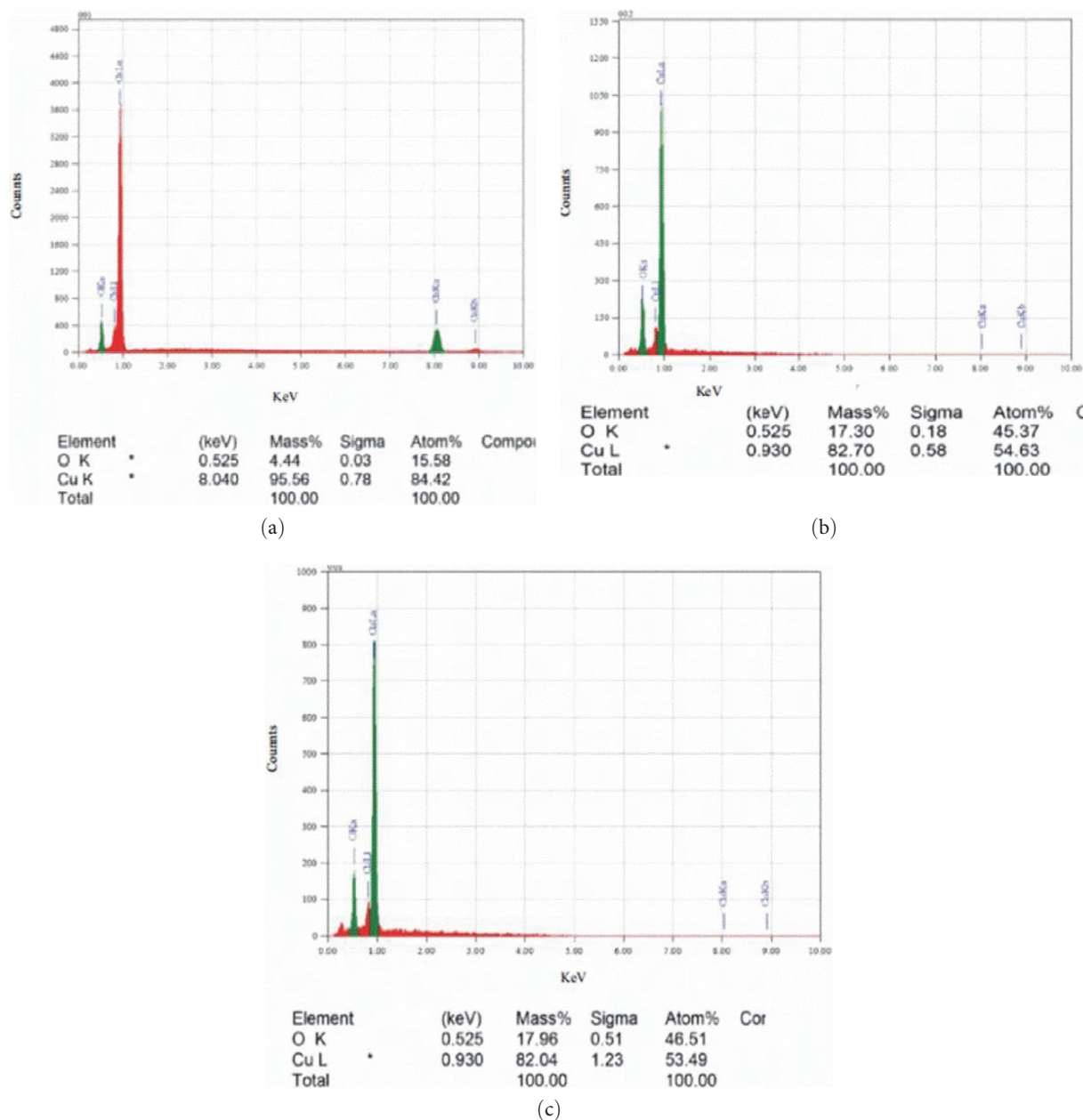
| Element | | (keV) | Mass% | Sigma | Atom% | Compo |
|---|---|---|---|---|---|---|
| O K | * | 0.525 | 4.44 | 0.03 | 15.58 | |
| Cu K | * | 8.040 | 95.56 | 0.78 | 84.42 | |
| Total | | | 100.00 | | 100.00 | |

(a)

| Element | (keV) | Mass% | Sigma | Atom% | C |
|---|---|---|---|---|---|
| O K | 0.525 | 17.30 | 0.18 | 45.37 | |
| Cu L    * | 0.930 | 82.70 | 0.58 | 54.63 | |
| Total | | 100.00 | | 100.00 | |

(b)

| Element | (keV) | Mass% | Sigma | Atom% | Cor |
|---|---|---|---|---|---|
| O K | 0.525 | 17.96 | 0.51 | 46.51 | |
| Cu L    * | 0.930 | 82.04 | 1.23 | 53.49 | |
| Total | | 100.00 | | 100.00 | |

(c)

FIGURE 16: EDX pattern of CuO film electrodeposited at various potential values: (a) −0.45, (b) −0.50, and (c) −0.55 V.

can be less compact with cracks and also produces a microscopic crack which can make film fall off the substrate. The microscopic images of electrodeposited $Cu_2O$ thin film with various potential values in between −0.1 and −0.9 V was analyzed by Jiang et al. [62, 100] which is shown in Figure 14(a)–14(e). The influence of potential affected the agglomeration of particles with shape. As a result, the films deposited at −0.1, −0.3, and −0.5 V with respect to the reference electrode, the surface is made-up of regular, well-faced polyhedral crystallites Figure 14(a)–14(c), respectively. The applied voltage found to increase catholically; the films undergo a transformation from octahedral to cubic with agglomeration. The film deposited at −0.1 V versus SCE found to exhibits pyramid-shaped structure, as shown in Figure 14(a), whereas the film deposited at −0.3 V exhibits cubic structure (Figure 14(b)). The preferential orientation along (111) plane which has the highest oxygen atom density, rate of growth is found to be slow at lower deposition potential. The shape of $Cu_2O$ thus depends on the (111) crystal plane, resulting a pyramidal crystal surface with four faces (Figure 14(a)). The co-deposition with agglomeration Cu with cubic structure $Cu_2O$ when deposited at −0.5 V is in (Figure 14(c)) which is confirmed by XRD analysis. The deposition potential at −0.7 and −0.9 V is exhibit a granular spherical morphology in Figures 14(d) and 14(e) and the average diameter of the grains tends to be

~50 nm [62]. The SEM images of electrodeposition of CuO thin film at various deposition potentials in between 2 and 4 V [68] is shown in Figure 15(a)–15(c). The deposition potential at 2 V, the grains exhibit morphology of symmetrical flower-like CuO nanostructure as shown in Figure 15(a). The grain growth of CuO flower nanostructure is composed of the irregular nanorods with about 50 nm in width and 125 nm in length. As the deposition voltage increased, symmetrical star-like CuO nanostructures formed and the largest size of nanoparticles are about 125 nm in width and 150 nm in length, as shown in Figure 15(b). In general, there is a positive correlation between grain nucleation and growth and deposition voltage, which causes the size of the nanocrystals to increase. Figure 15(c) shows the appearance of micron-sized spheres made of nanoparticles when the voltage is equal to 4 V. This is due to the fact that at lower voltages, the growth rate along (002) planes are faster than that of other planes [68]. Sayem Rahman et al. [77] observed that the EDX analysis of CuO at different depositio potential in the range between −0.45 and 0.55 V (Figure 16(a)–16(c)) [77]. From this observation there is 4.44% of oxygen and 95.56% of copper presented deposition potential at −0.45 V. From this result, the deposited film not entirely converted cuprous or cupric oxide. The deposition potential at −0.50 V slightly oxygen content increased, as a result, 17.94% of oxygen and 82.06% of copper presented. The percentage value of oxygen in the cupric oxide is the result which is closer to the cupric oxide. The deposition potential −0.55 V, there is 17.95% of oxygen and 82.05% copper present in the sample. To become the result, the oxygen content 20.13% is very close to the cupric oxide.

## 7. Conclusion

The basics of electrodeposition with significant parameters such as potential, bath temperature, solution pH, and substrate nature for CuO and $Cu_2O$ thin films from alkaline and acidic bath were explained. The influence of potential values for CuO and $Cu_2O$ thin film and its growth, thickness, structure, morphology, and hydration were explained. The temperature of the electrolytic bath at 40°C, there is formation of film with poor crystallinity, whereas the films deposited at bath temperature up to 70°C have well-defined crystallinity. The solution pH maintained at lower value around $12.0 \pm 0.1$ there is a formation of $Cu_2O$, whereas the value increased above $12.5 \pm 0.5$ does not allow the formation of $Cu_2O$. The complexing agents maintain state of ions $Cu^{2+}$ in the electrolyte solution as well as self-decomposition of $Cu^{2+}$ ions. The annealing temperature with reducing agent (L+) tartaric acid maintained the formation of CuO. Structural properties of electrodeposited CuO found to exhibit monoclinic and cubic phase, whereas $Cu_2O$ exhibits cubic phase only. The surface morphology of CuO and $Cu_2O$ grain growth which exhibits cubic, pyramid, leaf, and cluster structures with various bath temperature, potential, and complexing agent. So, we have concluded that the electrodeposition of CuO and $Cu_2O$ thin films were easily triggered with the oxidation states, structural phase, and surface morphology with its reliability for recent applications.

## Data Availability

The data used to support the findings of this study are included in the article. Should further data or information be required, these are available from the corresponding author upon request.

## Conflicts of Interest

The authors declare that they have no conflicts of interest.

## References

[1] A. Akbari, M. Amini, A. Tarassoli, B. Eftekhari-Sis, N. Ghasemian, and E. Jabbari, "Transition metal oxide nanoparticles as efficient catalysts in oxidation reactions," *Nano-Structures & Nano-Objects*, vol. 14, pp. 19–48, 2018.

[2] Z. J. Deng, M. Liang, I. Toth, M. Monteiro, and R. F. Minchin, "Plasma protein binding of positively and negatively charged polymer-coated gold nanoparticles elicits different biological responses," *Nanotoxicology*, vol. 7, no. 3, pp. 314–322, 2013.

[3] A. K. Arora, V. S. Jaswal, K. Singh, and R. Singh, "Applications of metal/mixed metal oxides as photocatalyst: a review," *Oriental Journal of Chemistry*, vol. 32, no. 4, pp. 2035–2042, 2016.

[4] A. Muthuvel, M. Jothibas, and C. Manoharan, "Synthesis of copper oxide nanoparticles by chemical and biogenic methods: photocatalytic degradation and in vitro antioxidant activity," *Nanotechnology for Environmental Engineering*, vol. 5, Article ID 14, 2020.

[5] Y. Z. Lu, W. T. Wei, and W. Chen, "Copper nanoclusters: synthesis, characterization and properties," *Chines Science Bulletin*, vol. 57, pp. 41–47, 2012.

[6] R. Koutavarapu, M. R. Tamtam, M. C. Rao, S. G. Peera, and J. Shim, "Recent progress in transition metal oxide/sulfide quantum dots-based nanocomposites for the removal of toxic organic pollutants," *Chemosphere*, vol. 272, Article ID 129849, 2021.

[7] E. Mousali and M. A. Zanjanchi, "Electrochemical synthesis of copper(II) oxide nanorods and their application in photocatalytic reactions," *Journal of Solid State Electrochemistry*, vol. 23, pp. 925–935, 2019.

[8] F. Zhang, Y. An, W. Zhai et al., "Nanotubes within transition metal silicate hollow spheres: facile preparation and superior lithium storage performances," *Materials Research Bulletin*, vol. 70, pp. 573–578, 2015.

[9] H. Motahira, U. Sana, and I. S. Kim, "Copper oxide (CuO) loaded polyacrylonitrile (PAN) nanofiber membranes for antimicrobial breath mask applications," *Current Research in Biotechnology*, vol. 1, pp. 1–10, 2019.

[10] L. Chen, S. Shet, H. Tang et al., "Electrochemical deposition of copper oxidenanowires for photoelectrochemical applications," *Journal of Materials Chemistry*, vol. 20, no. 33, pp. 6962–6967, 2010.

[11] C. Wang, F. Yang, Y. Cao, X. He, Y. Tang, and Y. Li, "Cupric oxide nanowires on three-dimensional copper foam for application in click reaction," *RSC Advances*, vol. 7, no. 16, pp. 9567–9572, 2017.

[12] G. Altindemir and C. Gumus, "$Cu_2O$ thin films prepared by using four different copper salts at a low temperature: an

investigation of their physical properties," *Materials Science in Semiconductor Processing*, vol. 107, Article ID 104805, 2020.

[13] G. Salek, C. Tenailleau, P. Dufour, and S. Guillemet-Fritsch, "Room temperature inorganic polycondensation of oxide ($Cu_2O$ and ZnO) nanoparticles and thin films preparation by the dip-coating technique," *Thin Solid Films*, vol. 589, pp. 872–876, 2015.

[14] S. Ganguly, R. Jha, P. K. Guha, and C. Jacob, "Synthesis of CuO nanoflowers and their application towards inflammable gas sensing," *Journal of Electronic Materials*, vol. 49, pp. 5070–5076, 2020.

[15] T. Osaka, T. Nakanishi, S. Shanmugam, S. Takahama, and H. Zhang, "Effect of surface charge of magnetite nanoparticles on their internalization into breast cancer and umbilical vein endothelial cells," *Colloids and Surfaces B: Biointerfaces*, vol. 71, no. 2, pp. 325–330, 2009.

[16] J.-J. Young, C.-C. Chen, Y.-C. Chen et al., "Positively and negatively surface-charged chondroitin sulfate-trimethylchitosan nanoparticles as protein carriers," *Carbohydrate Polymers*, vol. 137, pp. 532–540, 2016.

[17] S. Jeon, J. Clavadetscher, D.-K. Lee, S. V. Chankeshwara, M. Bradley, and W.-S. Cho, "Surface charge-dependent cellular uptake of polystyrene nanoparticles," *Nanomaterials*, vol. 8, no. 12, Article ID 1028, 2018.

[18] D. Mundekkad and W. C. Cho, "Nanoparticles in clinical translation for cancer therapy," *International Journal of Molecular Sciences*, vol. 23, no. 3, Article ID 1685, 2022.

[19] H. Chen and L. Wang, "Nanostructure sensitization of transition metal oxides for visible-light photocatalysis," *Beilstein Journal of Nanotechnology*, vol. 5, pp. 696–710, 2014.

[20] Y. Tang, Z. Qin, S. Yin, and H. Sun, "Transition metal oxide and chalcogenide-based nanomaterials for antibacterial activities: an overview," *Nanoscale*, vol. 13, no. 13, pp. 6373–6388, 2021.

[21] A. D. Karthik and K. Geetha, "Applications of transition metal nanoparticles in antimicrobial therapy," *Biomaterials and Tissue Engineering Bulletin*, vol. 3, no. 1–4, pp. 28–34, 2016.

[22] C. Prabukumar, S. Meti, and U. K. Bhat, "Enhancing the electrochemical performance of ZnO anode by novel additive of $MoS_2$–$SnO_2$ nanocomposite for the zinc alkaline battery application," *Journal of Materials Science: Materials in Electronics*, vol. 33, pp. 2534–2549, 2022.

[23] W. Qian, Z. Chen, S. Cottingham et al., "Surfactant-free hybridization of transition metal oxidenanoparticles with conductive graphene for high-performance supercapacitor," *Green Chemistry*, vol. 14, no. 2, pp. 371–377, 2012.

[24] S. Tachikawa, A. Noguchi, T. Tsuge, M. Hara, O. Odawara, and H. Wada, "Optical properties of ZnO nanoparticles capped with polymers," *Materials*, vol. 4, no. 6, pp. 1132–1143, 2011.

[25] X. Lü, W. Yang, Z. Quan et al., "Enhanced electron transport in Nb-doped $TiO_2$ nanoparticles via pressure-induced phase transitions," *Journal of the American Chemical Society*, vol. 136, no. 1, pp. 419–426, 2014.

[26] O. Takeda, T. Ouchi, and T. H. Okabe, "Recent progress in titanium extraction and recycling," *Metallurgical and Materials Transactions B*, vol. 51, pp. 1315–1328, 2020.

[27] S. Shen, J. Chen, M. Wang et al., "Titanium dioxide nanostructures for photoelectrochemical applications," *Progress in Materials Science*, vol. 98, pp. 299–385, 2018.

[28] M. Arif, A. Sanger, and A. Singh, "Sputter deposited chromium nitride thin electrodes for supercapacitor applications," *Materials Letters*, vol. 220, pp. 213–217, 2018.

[29] S. M. Ansari, M. Zubair Khan, H. Anwar et al., "Tungsten oxide-reduced graphene oxide composites for photoelectrochemical water splitting," *Arabian Journal for Science and Engineering*, vol. 46, pp. 813–825, 2021.

[30] S. Saini, A. Joshi, and P. Chand, "Recent advancement in tungsten oxide as an electrode material for supercapacitor applications," in *Renewable Energy Towards Smart Grid*, vol. 823 of *Lecture Notes in Electrical Engineering*, pp. 327–334, Singapore, 2022.

[31] Y. A. Taya, H. M. Ali, E. K. Shokr et al., "Mn-doped molybdenum trioxide for photocatalysis and solar cell applications," *Optical Materials*, vol. 12, Article ID 111614, 2021.

[32] L. Gnanasekaran, R. Hemamalini, S. Rajendran et al., "Nanosized $Fe_3O_4$ incorporated on a $TiO_2$ surface for the enhanced photocatalytic degradation of organic pollutants," *Journal of Molecular Liquids*, vol. 287, Article ID 110967, 2019.

[33] M. M. de Góis, W. de Paiva Araújo, R. B. da Silva, G. E. da Luz Jr., and J. M. Soares, "$Bi_{25}FeO_{40}$–$Fe_3O_4$–$Fe_2O_3$ composits: synthesiss structursal characterization, mgnetic and UV–visible photocatalytic propertied," *Journal of Alloys and Compounds*, vol. 785, pp. 598–602, 2019.

[34] A. Chouchaine, S. Kouass, F. Touati, N. Amdouni, and H. Dhaouadi, "$Fe_3O_4$ nanomaterials: synthesis, optical and electrochemical propertie," *Journal of the Australian Ceramic Society*, vol. 57, pp. 469–477, 2021.

[35] G.-S. Jang, S. Ameen, M. Shaheer Akhtar, and H.-S. Shin, "Cobalt oxide nanocubes as electrode material for the performance evaluation of electrochemical supercapacitor," *Ceramics International*, vol. 44, no. 1, pp. 588–595, 2018.

[36] X. Sun, H. Liu, G. Xu, J. Bai, and C. Li, "Embedding $Co_2P$ nanoparticles into N&P co-doped carbon fibers for hydrogen evolution reaction and supercapacitor," *International Journal of Hydrogen Energy*, vol. 46, no. 2, pp. 1560–1568, 2021.

[37] N. A. Mala, M. A. Dar, S. Sivakumar, K. S. Bhat, G. N. Sinha, and K. M. Batoo, "Electrochemical supremacy of cobalt-doped nickel oxide and its supercapacitor applications with its mesoporous morphology," *Journal of Materials Science: Materials in Electronics*, vol. 33, pp. 11582–11590, 2022.

[38] M.-Y. Liu, J.-Y. Wang, L. Duan, X. Liu, and L. Zhang, "Nickel oxide modified $C_3N_5$ photocatalyst for enhanced hydrogen evolution performance," *Journal of Fuel Chemistry and Technology*, vol. 50, no. 2, pp. 243–249, 2022.

[39] S. Mahboob, R. Nivetha, K. Gopinath et al., "Facile synthesis of gold and platinum doped titanium oxide nanoparticles for antibacterial and photocatalytic activity: a photodynamic approach," *Photodiagnosis and Photodynamic Therapy*, vol. 33, Article ID 102148, 2021.

[40] A. Bhaumik, A. Haque, P. Karnati, M. F. N. Taufique, R. Patel, and K. Ghosh, "Copper oxide based nanostructures for improved solar cell efficiency," *Thin Solid Films*, vol. 572, pp. 126–133, 2014.

[41] A. Ullah, M. Saadullah, F. Alvi et al., "Synergistic effect of silver doped ZnO nanomaterials enhances the anticancer potential against A459 lung cancer cells," *Journal of King Saud University-Science*, vol. 34, no. 1, Article ID 101724, 2022.

[42] Y. Xia, L. He, J. Feng, S. Xu, L. Yao, and G. Pan, "Waterproof and moisture-permeable polyurethane nanofiber membrane with high strength, launderability, and durable antimicrobial properties," *Nanomaterials*, vol. 12, no. 11, Article ID 1813, 2022.

[43] N. Kunthakudee, T. Puangpetch, P. Ramakul, K. Serivalsatit, and M. Hunsom, "Light-assisted synthesis of Au/$TiO_2$ nanoparticles

for H$_2$ production by photocatalytic water splitting," *International Journal of Hydrogen Energy*, vol. 47, no. 56, pp. 23570–23582, 2022.

[44] F. Yi, J. B. DeLisio, N. Nguyen, M. R. Zachariah, and D. A. LaVan, "High heating rate decomposition dynamics of copper oxide by nanocalorimetry-coupled time-of-flight mass spectrometry," *Chemical Physics Letters*, vol. 689, pp. 26–29, 2017.

[45] R. Bunea, A. K. Saikumar, and K. Sundaram, "A comparison of optical properties of CuO and Cu$_2$O thin films for solar cell applications," *Materials Sciences and Applications*, vol. 12, no. 7, pp. 315–329, 2021.

[46] J. Salas-Leiva, G. Herrera-Pérez, L. Palma-Cano, G. Rojas-George, C. Ornelas-Gutierrez, and A. Luna-Velasco, "Structural and microstructural analysis for CuO nanoparticles prepared by precipitation method," *Microscopy and Microanalysis*, vol. 25, no. S2, pp. 1984-1985, 2019.

[47] V. Dhanasekaran, T. Mahalingam, R. Chandramohan, J.-K. Rhee, and J. P. Chu, "Electrochemical deposition and characterization of cupric oxide thin films," *Thin Solid Films*, vol. 520, no. 21, pp. 6608–6613, 2012.

[48] P. Steiner, S. Hüfner, A. Jungmann, V. Kinsinger, and I. Sander, "Photoemission valence band spectra and electronic density of states in copper oxides and copper based ceramic super-conductors," *Zeitschrift für Physik B Condensed Matter*, vol. 74, pp. 173–182, 1989.

[49] T. Ikenoue, T. Kawai, R. Wakashima, M. Miyake, and T. Hirato, "Hole mobility improvement in Cu$_2$O thin films prepared by the mist CVD method," *Applied Physics Express*, vol. 12, no. 5, Article ID 055509, 2019.

[50] P. Poizot, C.-J. Hung, M. P. Nikiforov, E. W. Bohannan, and J. A. Switzer, "An electrochemical method for CuO thin film deposition from aqueous solution," *Electrochemical and Solid-State Letters*, vol. 6, no. 2, pp. C21–C25, 2003.

[51] J.-H. Park, T. Hagio, Y. Kamimoto, and R. Ichino, "The effect of bath pH on electrodeposition and corrosion properties of ternary Fe–W–Zn alloy platings," *Journal of Solid State Electrochemistry*, vol. 25, pp. 1901–1913, 2021.

[52] S. Ghosh and S. Roy, "Electrochemical copper deposition from an ethaline-CuCl$_2$·2H$_2$O DES," *Surface and Coatings Technology*, vol. 238, pp. 165–173, 2014.

[53] V. D. Patake, S. S. Joshi, C. D. Lokhande, and O.-S. Joo, "Electrodeposited porous and amorphous copper oxide film for application in supercapacitor," *Materials Chemistry and Physics*, vol. 114, no. 1, pp. 6–9, 2009.

[54] H. Rahal, R. Kihal, A. M. Affoune, and S. Rahal, "Effect of solution pH on properties of cuprous oxide thin films prepared by electrodeposition from a new bath," *Journal of Electronic Materials*, vol. 49, pp. 4385–4391, 2020.

[55] I. S. Brandt, M. A. Tumelero, S. Pelegrini, G. Zangari, and A. A. Pasa, "Electrodeposition of Cu$_2$O: growth, properties, and applications," *Journal of Solid State Electrochemistry*, vol. 21, pp. 1999–2020, 2017.

[56] B. Beverskog and I. Puigdomenech, "Revised pourbaix diagrams for copper at 25 to 300°C," *Journal of The Electrochemical Society*, vol. 144, no. 10, Article ID 3476, 1997.

[57] Y.-J. Oh, G.-S. Park, and C.-H. Chung, "Planarization of copper layer for damascene interconnection by electrochemical polishing in alkali-based solution," *Journal of the Electrochemical Society*, vol. 153, no. 7, Article ID G617, 2006.

[58] J. Gambino, J. Robbins, T. Rutkowski et al., "Etching of copper in deionized water rinse," in *2008 15th International Symposium on the Physical and Failure Analysis of Integrated Circuits*, pp. 1–8, IEEE, 2008.

[59] J. Kanakaraj and H. B. Ramalingam, "Effect of electrolytic bath temperature on magnetic and structural properties of electrodeposited NiFeW nano crystalline thin films," *Oriental Journal of Chemistry*, vol. 33, no. 6, pp. 2899–2904, 2017.

[60] M. Keikhaei and M. Ichimura, "Fabrication of copper oxide thin films by galvanostatic deposition from weakly acidic solutions," *International Journal of Electrochemical Science*, vol. 13, pp. 9931–9941, 2018.

[61] M. Benhaliliba, D. Mohra, and M. Serin, "Effect of electrochemical bath temperature on Cu$_2$O/ITO device properties," *Advanced Science, Engineering and Medicine*, vol. 11, no. 6, pp. 519–524, 2019.

[62] X. Jiang, M. Zhang, S. Shi, G. He, X. Song, and Z. Sun, "Microstructure and optical properties of nanocrystalline Cu$_2$O thin films prepared by electrodeposition," *Nanoscale Research Letters*, vol. 9, Article ID 219, 2014.

[63] C. Ravichandiran, A. Sakthivelu, R. Davidprabu et al., "Effect of deposition temperature on key optoelectronic properties of electrodeposited cuprous oxide thin films," *Optical and Quantum Electronics*, vol. 50, Article ID 281, 2018.

[64] M. A. Hossain, R. Al-Gaashani, H. Hamoudi et al., "Controlled growth of Cu$_2$O thin films by electrodeposition approach," *Materials Science in Semiconductor Processing*, vol. 63, pp. 203–211, 2017.

[65] C. Zhu, A. Osherov, and M. J. Panzer, "Surface chemistry of electrodeposited Cu$_2$O films studied by XPS," *Electrochimica Acta*, vol. 111, pp. 771–778, 2013.

[66] Q.-B. Ma, J. P. Hofmann, A. Litke, and E. J. M. Hensen, "Cu$_2$O photoelectrodes for solar water splitting: Tuning photoelectrochemical performance by controlled faceting," *Solar Energy Materials and Solar Cells*, vol. 141, pp. 178–186, 2015.

[67] Z. Zhang, W. Hu, Y. Deng et al., "The effect of complexing agents on the oriented growth of electrodeposited microcrystalline cuprous oxide film," *Materials Research Bulletin*, vol. 47, no. 9, pp. 2561–2565, 2012.

[68] Y. Wang, T. Jiang, D. Meng et al., "Fabrication of nanostructured CuO films by electrodeposition and their photocatalytic properties," *Applied Surface Science*, vol. 317, pp. 414–421, 2014.

[69] T. Mahalingam, J. S. P. Chitra, S. Rajendran, and P. J. Sebastian, "Potentiostatic deposition and characterization of Cu$_2$O thin films," *Semiconductor Science and Technology*, vol. 17, no. 6, Article ID 565, 2002.

[70] W. Zhao, W. Fu, H. Yang et al., "Electrodeposition of Cu$_2$O films and their photoelectrochemical properties," *CrystEngComm*, vol. 13, no. 8, pp. 2871–2877, 2011.

[71] A. E. Rakhshani and J. Varghese, "Potentiostatic electrodeposition of cuprous oxide," *Thin Solid Films*, vol. 157, no. 1, pp. 87–96, 1988.

[72] P. A. Praveen Janantha, L. N. L. Perera, K. M. D. C. Jayathilakab, J. K. D. S. Jayanetti, D. P. Dissanayakaa, and W. P. Siripalab, "Use of Cu$_2$O microcrystalline thin film semiconductors for gas sensing," *Proceedings of the Technical Sessions*, vol. 25, pp. 70–76, 2009.

[73] V. Dhanasekaran, T. Mahalingam, S. Rajendran, J. K. Rhee, and D. Eapen, "Electroplated CuO thin films from high alkaline solutions," *Journal of New Materials for Electrochemical Systems*, vol. 15, no. 1, pp. 49–55, 2012.

[74] O. Fasakin, M. A. Eleruja, O. O. Akinwunmi, B. Olofinjana, E. Ajenifuja, and E. O. B. Ajayi, "Synthesis and characterization of metal organic chemical vapour deposited copper

titanium oxide (Cu-Ti-O) thin films from single solid source precursor," *Journal of Modern Physics*, vol. 4, no. 12C, pp. 1–6, 2013.

[75] K. P. Muthe, J. C. Vyas, S. N. Narang et al., "A study of the CuO phase formation during thin film deposition by molecular beam epitaxy," *Thin Solid Films*, vol. 324, no. 1-2, pp. 37–43, 1998.

[76] J. P. Enríquez and X. Mathew, "Influence of the thickness on structural, optical and electrical properties of chemical bath deposited CdS thin films," *Solar Energy Materials and Solar Cells*, vol. 76, no. 3, pp. 313–322, 2003.

[77] A. S. M. Sayem Rahman, M. A. Islam, and K. M. Shorowordi, "Electrodeposition and characterization of copper oxide thin films for solar cell applications," *Procedia Engineering*, vol. 105, pp. 679–685, 2015.

[78] W. Simka, D. Puszczyk, and G. Nawrat, "Electrodeposition of metals from non-aqueous solutions," *Electrochimica Acta*, vol. 54, no. 23, pp. 5307–5319, 2009.

[79] H. Rahal, R. Kihal, A. M. Affoune, and S. Rahal, "Electrodeposition and characterization of $Cu_2O$ thin films using sodium thiosulfate as an additive for photovoltaic solar cells," *Chinese Journal of Chemical Engineering*, vol. 26, no. 2, pp. 421–427, 2018.

[80] R. Oommen, U. Rajalakshmi, and Sanjeeviraja, "Characteristics of electron beam evaporated and electrodeposited $Cu_2O$ thin films–comparative study," *International Journal of Electrochemical Science*, vol. 7, pp. 8288–8298, 2012.

[81] K. P. Ganesan, G. Sivakumar, N. Anandhan, T. Marimuthu, R. Panneerselvam, and A. Amali Roselin, "Influence of bath temperatures on physical and electrical properties of potentiostatically deposited $Cu_2O$ thin films for heterojunction solar cell applications," *Optical and Quantum Electronics*, vol. 51, Article ID 37, 2019.

[82] E. S. Güler, *Effects of Electroplating Characteristics on the Coating Properties*, InTech, 2016.

[83] S. Thanikaikarasan, R. Perumal, K. Sankaranarayanan, and T. Mahalingam, "Electrochemical, microstructural, compositional and optical characterization of copper oxide and copper sulfide thin films," *Journal of Materials Science: Materials in Electronics*, vol. 29, pp. 15529–15534, 2018.

[84] A. Maciej, N. Łatanik, M. Sowa, I. Matuła, and W. Simka, "Electrodeposition of copper and brass coatings with olive-like structureb," *Materials*, vol. 14, no. 7, Article ID 1762, 2021.

[85] A. I. Inamdar, S. H. Mujawar, S. R. Barman, P. N. Bhosale, and P. S. Patil, "The effect of bath temperature on the electrodeposition of zinc oxide thin films via an acetate medium," *Semiconductor Science and Technology*, vol. 23, no. 8, Article ID 085013, 2008.

[86] L. Mentar, H. Lahmar, M. R. Khelladi, and A. Azizi, "The effect of bath temperature on the electrodeposition of zinc oxide nanostructures via nitrates solution," *Journal of New Technology and Materials*, vol. 4, no. 1, pp. 41–45, 2014.

[87] Z. Zainal, A. Kassim, M. Z. Hussein, and C. H. Ching, "Effect of bath temperature on the electrodeposition of copper tin selenide films from aqueous solution," *Materials Letters*, vol. 58, no. 16, pp. 2199–2202, 2004.

[88] C. K. Ko and W. G. Lee, "Effects of pH variation in aqueous solutions on dissolution of copper oxide," *Surface and Interface Analysis*, vol. 42, no. 6-7, pp. 1128–1130, 2010.

[89] Y. Wang, K. Li, X. Chen, and H. Zhou, "Responses of microbial community to pH stress in bioleaching of low grade copper sulfide," *Bioresource Technology*, vol. 249, pp. 146–153, 2018.

[90] K. Jrajri, M. Beraich, I. Warad, A. Guenbour, A. Bellaouchou, and A. Zarrouk, "Electrodeposition of $Cu_2O$ thin film onto copper substrate by linear sweep voltammetry at low duration: effect of bath pH," *Biointerface Research in Applied Chemistry*, vol. 12, no. 6, pp. 7715–7724, 2022.

[91] İ. H. Karahan, "Effects of pH value of the electrolyte and glycine additive on formation and properties of electrodeposited Zn-Fe coatings," *Scientific World Journal*, vol. 2013, Article ID 273953, 7 pages, 2013.

[92] H. X. Yang, Z. L. Song, Y. W. Song, and H. Zhang, "Effect of pH value on the electrodeposition potential of Cu-In alloy film," *Key Engineering Materials*, vol. 373-374, pp. 216–219, 2008.

[93] W. Wu, N. Eliaz, and E. Gileadi, "The effects of pH and temperature on electrodeposition of Re-Ir-Ni coatings from aqueous solutions," *Journal of the Electrochemical Society*, vol. 162, no. 1, pp. D20–D26, 2015.

[94] M. Nowicki and K. Wandelt, "Encyclopedia of interfacial chemistry," in *Encyclopedia of Interfacial Chemistry: Surface Science and Electrochemistry*, pp. 108–128, Elsevier, 2018.

[95] M. S. Safavi, F. C. Walsh, M. A. Surmeneva, R. A. Surmenev, and J. Khalil-Allafi, "Electrodeposited hydroxyapatite-based biocoatings: recent progress and future challenges," *Coatings*, vol. 11, no. 1, Article ID 110, 2021.

[96] K. Jrajri, M. Beraich, I. Warad, A. Guenbour, A. Bellaouchou, and A. Zarrouk, "Electrodeposition of $Cu_2O$ thin film onto the copper substrate by linear sweep voltammetry at low duration: effect of bath pH," *Biointerface Research in Applied Chemistry*, vol. 12, no. 6, pp. 7715–7724, 2022.

[97] S. Laidoudi, A. Y. Bioud, A. Azizi et al., "Growth and characterization of electrodeposited $Cu_2O$ thin films," *Semiconductor Science and Technology*, vol. 28, no. 11, Article ID 115005, 2013.

[98] A. Mahmood, F. Tezcan, and G. Kardaş, "Photoelectrochemical characteristics of CuO films with different electrodeposition time," *International Journal of Hydrogen Energy*, vol. 42, no. 36, pp. 23268–23275, 2017.

[99] M.-C. Huang, T. H. Wang, W.-S. Chang et al., "Temperature dependence on p-$Cu_2O$ thin film electrochemically deposited onto copper substrate," *Applied Surface Science*, vol. 301, pp. 369–377, 2014.

[100] X. Jiang, Q. Lin, M. Zhang, X. Song, and Z. Sun, "Effect of temperature and additive on the structural, morphological and optical properties of $Cu_2O$ thin films," *Optik*, vol. 126, no. 24, pp. 5544–5547, 2015.